

# A Value of Information-based assessment of strain-based thickness loss monitoring in ship hull structures

Nicholas E. Sillionis<sup>a,\*</sup>, Konstantinos N. Anyfantis<sup>a</sup>

<sup>a</sup>*Ship-Hull Structural Health Monitoring (S-H SHM) Group, School of Naval Architecture and Marine Engineering, National Technical University of Athens, 9 Heroon Polytechniou Av., Athens, 15780 Zografos, Greece*

---

## Abstract

Recent advances in Structural Health Monitoring (SHM) have attracted industry interest, yet real-world applications, such as in ship structures, remain scarce. Despite SHM's potential to optimise maintenance, its adoption in ships is limited due to the lack of clearly quantifiable benefits for hull maintenance. This study employs a Bayesian pre-posterior decision analysis to quantify the value of information (VoI) from SHM systems monitoring corrosion-induced thickness loss (CITL) in ship hulls, in a first-of-its kind analysis for ship structures. We define decision-making consequence cost functions based on exceedance probabilities relative to a target CITL threshold, which can be set by the decision-maker. This introduces a practical aspect to our framework, that enables implicitly modelling the decision-maker's risk perception. We apply this framework to a large-scale, high-fidelity numerical model of a commercial vessel and examine the relative benefits of different CITL monitoring strategies, including strain-based SHM and traditional on-site inspections.

**Keywords:** Value of information, Bayesian decision theory, Ship hull structures, Structural Health Monitoring, Condition-based maintenance

---

## 1. Introduction

Over the past decades, significant advances have been made in SHM-related research by capitalising on the simultaneous developments in sensing technology and the increase in processing power. Although the potential of SHM has been recognised by stakeholders across various engineering disciplines, industrial application at scale is still at a nascent stage. The shipping industry is a typical example; in recent years key stakeholders—primarily classification societies [1–3]—have viewed the potential offered by SHM to optimise maintenance planning as highly promising and thus included it in their strategic goals. Despite this interest, real-world installations of SHM systems are still quite rare and are typically found in non-civilian vessels [4]. Even then, the scope of these systems is confined to monitoring stresses on the ship hull and providing alarms if certain threshold values have been exceeded. Using structural response data to aid in decision-making or to optimise vessel operation and maintenance (O&M) remains largely a research topic [5].

Current hull structural maintenance practices revolve around a series of inspections that take place at fixed intervals. These are conventionally referred to as hull surveys and occur every 1,

---

\*Corresponding author.

Email addresses: [nsil@naval.ntua.gr](mailto:nsil@naval.ntua.gr) (Nicholas E. Sillionis), [kanyf@naval.ntua.gr](mailto:kanyf@naval.ntua.gr) (Konstantinos N. Anyfantis)

3 and 5 years, as mandated by regulations promulgated by certified authorities, i.e., classification societies. The timing of these inspections, and the actions that take place during each one, are precisely defined by class rules. In the case of bulk carriers and oil tankers, these rules conform to a unified standard set by the International Association of Classification Societies (IACS) [6, 7]. During these surveys different locations of the hull structure, which are considered prone to specific types of deterioration, e.g., CITL or fatigue cracking, are inspected either visually or through non-destructive testing (NDT) methods, e.g., ultrasonic thickness measurement. Locations that are mostly inaccessible during operation, e.g., water ballast tanks in the double bottom of the vessel, are inspected less frequently, i.e., during the 5-year survey when the vessel is in dry-dock. However, structural components in these locations are expected to suffer significant deterioration, especially CITL, due to their hostile operational environment, characterised by high salinity and significant temperature variation.

The combination of potentially severe CITL-related deterioration, relative inaccessibility, and infrequent inspection has driven research interest towards condition-based maintenance. In this setting, knowledge about the evolution of structural deterioration is used to flexibly schedule maintenance actions according to the (predicted) state of the structure at a given moment in time. Several, particularly earlier, works involved applying statistical methods to describe CITL, using historical data collected from operating vessels. These methods included using classic regression techniques to fit models that describe CITL evolution in time, such as the modified linear model proposed by Paik et al. [8], or the exponential-type models proposed by Garbatov et al. [9] and Qin et al. [10]. More recently, Bayesian inference has been used to obtain probabilistic variants of these models [11, 12], which enable uncertainty quantification (UQ), and are thus better suited for decision support, compared to deterministic point predictors.

Models fit on historical data may often be ill-suited to inform decision support, especially for newly built structures. Variations in operational conditions or structural design, among other factors, may render models that accurately explain deterioration in older structural systems unfit for newer ones. Certain conditions, related to both data collection and model selection, must be met to successfully transfer knowledge between structural systems. This is still an active area of research and is closely related to population-based SHM [13–15]. When it comes to CITL in ship hulls, the quantity and quality of data available to interested parties may pose a significant challenge to population-based methods, e.g., as evidenced by the significant uncertainty in CITL measurements reported in Paik et al. [8].

This fact, combined with the inability to frequently access enclosed spaces to collect CITL data, has led researchers to investigate the potential of indirect CITL monitoring. This constitutes a classic SHM task, which is typically achieved using structural response data, e.g., strains measured at particular locations of interest. In previous works, the authors used static strain data to detect the presence of CITL in both simplified structural components [16] and realistic hull structures [17] subjected to stochastic loading. Ghasemzadeh et al. [18, 19] have used the inverse finite element method (iFEM)—which is strain-based by definition—to identify pitting corrosion in steel structural components used in marine applications.

These works demonstrate that SHM is a feasible option when it comes to remote, indirect detection, and potentially prediction, of CITL. However, they do not fully demonstrate that it can be a feasible alternative for hull structural maintenance planning against CITL deterioration, since they offer no insight on the benefits of investing in and choosing SHM, as opposed to traditional maintenance strategies. This is a salient question, not only for marine structures, but for SHM

in general. Researchers have attempted to answer it by primarily employing notions of Bayesian decision theory; namely, the concept of the value of information (VoI) [20–26].

The VoI offers a rational framework for estimating the expected capital gains from incorporating an information acquisition strategy, such as conventional inspections or continuous monitoring, on an existing structure. Put simply, it seeks to estimate the cost savings achieved by using monitoring information to aid decision-making for the O&M of a structure. If these savings are greater than the intrinsic cost of the information acquisition strategy, as well as any potential maintenance or other costs related to it, then incorporating the strategy can be considered as beneficial.

As a result, the VoI has been widely used for SHM applications on a variety of engineering structures. The majority of works, including the origins of the use of the VoI in SHM, is related to civil infrastructure. Zonta et al. [21]—in one of the earliest works on the topic—demonstrated the use of the VoI to determine the impact of monitoring on the management of a pedestrian bridge subjected to potentially critical damages. Kamariotis et al. [27, 28] and Giordano et al. [29] used the VoI to assess the effect of monitoring information on the management of scoured bridges, while Chadha et al. [30–32] employed it on a case study based on a navigation lock miter gate. Beyond civil infrastructure, Nielsen et al. [33] applied the VoI on a case study related to risk-based maintenance of an operating wind turbine blade; Cantero-Chinchilla et al. [34] used the VoI in an optimal sensor placement context for ultrasonic guided-wave SHM of aluminium aeronautical structural components.

To the authors’ knowledge, this is the first time that a comprehensive assessment of the value offered by SHM to hull structural maintenance has been undertaken. Our objective is to demonstrate a methodology with which stakeholders can translate their interest in SHM or CBM to actionable information to support their decision to invest. Thus, we view this work as a necessary step towards the practical implementation of SHM for ship hulls. To achieve this objective, we will use the VoI to quantify the expected reward obtained by using different potential SHM strategies to monitor a typical form of slowly evolving deterioration found in ship hull structures, namely CITL. We employ a pre-posterior decision analysis to quantify the VoI, which requires casting the problem of CITL monitoring as one of Bayesian model updating (BMU). Necessary (synthetic) strain data is generated using a high-fidelity finite element (FE) model of part of a ship hull structure that was previously developed by the authors [17]. The VoI is quantified using the alternative definition proposed in Chadha et al. [30], i.e., the expected reward to investment risk ratio.

We propose a modified version of the linear consequence cost functions for the binary decision setting found in the original [30]. We define costs using an exceedance probability estimate, as opposed to a state variable, i.e., a quantity directly describing the level of deterioration. The proposed exceedance probability is defined with respect to a threshold value set by the decision-maker, which could reflect a level of deterioration that is important in the context of maintenance planning. This definition provides an additional link to practical decision-making settings, while also implicitly modelling risk perception through the choice of threshold. Due to a lack of available information, the consequence costs have been defined in normalised form, between 0 and 1, with extreme values chosen using rational considerations.

The VoI was quantified for different—in terms of the BMU problem definition—SHM strategies for various decision settings. The VoI was compared across the different strategies, as well as with the VoI estimate for a scenario involving a typical on-site inspection. In addition to the various decision settings, the effect of different decision-making (extrinsic) and system-related (intrinsic) cost assignments was investigated to determine, at least qualitatively, cost levels that justify investment

in SHM. The rest of the paper is structured as follows: key theoretical principles used to quantify the VoI from CITL monitoring are presented in Section 2. The employed case study is described in Section 3. Section 4 presents results from the numerical implementation of the framework and is followed by concluding remarks in Section 5.

## 2. Quantifying the value of information from CITL monitoring

This section presents the main elements required to quantify the VoI from CITL monitoring. First, we provide a brief overview of BMU, focusing on the problem of interest here. Then, we define the VoI and discuss the decision setting for CITL monitoring that has been used to define decision-making consequence cost functions. Finally, we provide an overview of the computational implementation of the proposed framework.

### 2.1. Bayesian model updating for CITL monitoring

Let us begin by considering that the quantity of interest (QoI) in this work, i.e., CITL at a specific region of the hull structure, is a random variable (RV)  $\Delta\mathcal{T} : \Omega_{\Delta\mathcal{T}} \rightarrow \mathbb{R}$ . According to this notation,  $\Omega_{\Delta\mathcal{T}}$  refers to the sample space of the RV, which is real-valued, i.e., a scalar with realisations  $\Delta\tau \in \mathbb{R}$ . In turn, this implies that we consider uniform thickness loss over the region of interest. Generally, we are interested in monitoring CITL for an extended period of time after its onset, i.e., the moment when the protective coating fails. This is reasonable, since monitoring the evolution of deterioration can help make timely maintenance decisions, which could minimise downtime and reduce related costs, as well as control the maintenance costs associated with a potential repair.

Therefore, we require a model to describe the evolution of CITL through time. Let us denote the operator that describes this model as  $\mathcal{F}$ . Then,  $\mathcal{F}(t; \boldsymbol{\theta})$  is a stochastic model parametrised with respect to a random vector  $\boldsymbol{\theta} \in \mathbb{R}^{d_\theta}$ , where  $d_\theta$  refers to the number of model parameters. Deteriorating structural systems can be considered as a class of dynamical systems, and can thus be described using a stochastic state space representation [35]. In this setting,  $\mathcal{F}(t; \boldsymbol{\theta})$  represents the state model, and  $\Delta\tau$  is the state variable. To fully cast the problem in this form, we write:

$$\Delta\tau_k = \mathcal{F}(t_k; \boldsymbol{\theta}) + \psi \quad (1)$$

$$\mathbf{y}_k = \mathcal{H}(\Delta\tau_k; \boldsymbol{\phi}) + \boldsymbol{\xi} \quad (2)$$

In Eqs. (1) & (2), time has been expressed in discrete form with  $\{t_k\}_{k=1}^K$  consisting of the instants when measurements become available. In Eq. (1), the term  $\psi$  is a random variable known typically as the process noise, which summarises the (epistemic) uncertainty related to the state model. In Eq. (2), the operator  $\mathcal{H}$  is known as the observation or measurement model, which is also—in principle—a stochastic model parametrised by a random vector  $\boldsymbol{\phi} \in \mathbb{R}^{d_\phi}$ . This operator maps the state variable, which may not be directly observable, to an observable space. The observations of the system, described by the vector  $\mathbf{y}_k \in \mathbb{R}^N$ , are viewed as noisy outputs of the observation model. The additive random vector  $\boldsymbol{\xi} \in \mathbb{R}^N$  describes the observation noise, and quantifies aleatoric uncertainty.

The state-space formulation described through Eqs. (1) & (2) is ideal for SHM purposes, since it provides a general structure to define BMU problems for different inferential QoIs and types of available observations. Figure 1 contains a graphical representation—in the form of directed graphical

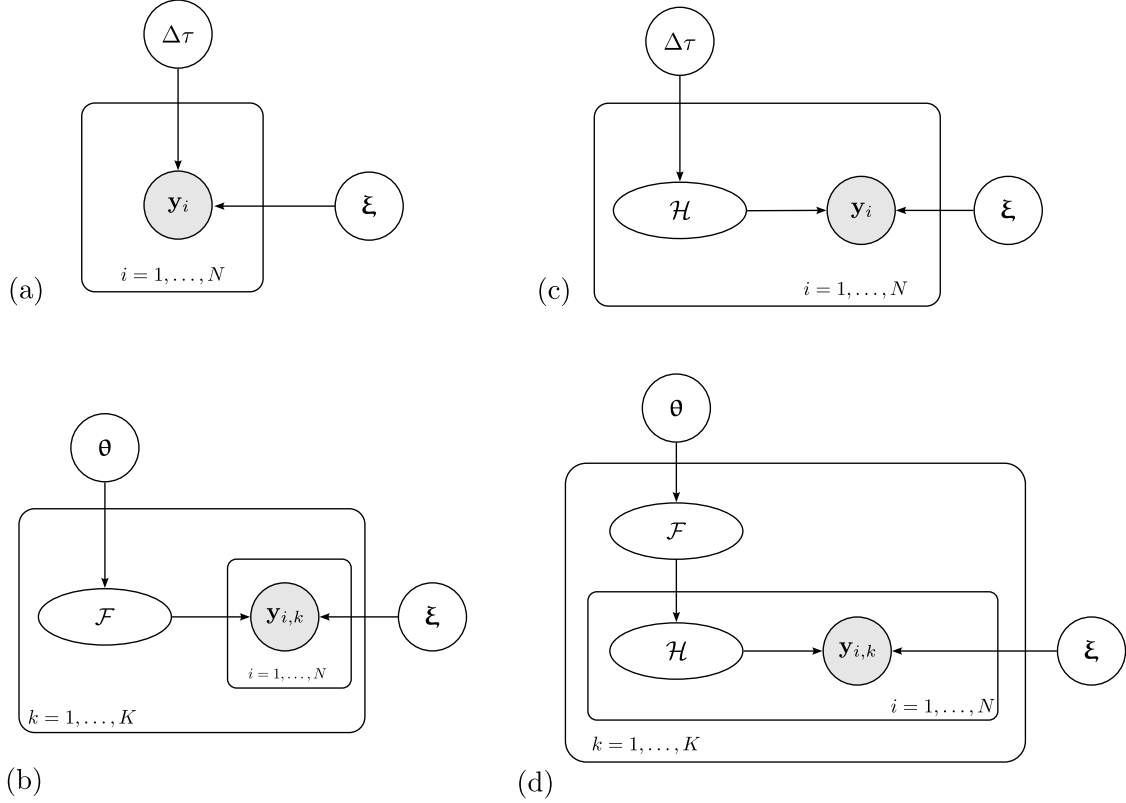


Figure 1: Directed graphical models (DGMs) of BMU problems considered for CITL monitoring.

models (DGMs)—of the BMU problems that will be treated in the context of this work. Circular empty nodes denote RVs that are learnt during inference; grey shaded nodes denote observed quantities; ovals denote transformations of random variables. The direction of arrows between RVs implies conditional relationships, while the plates iterating over  $k$ , i.e., the time dimension, and  $i$ , i.e., the feature dimension, indicate a conditionally independent structure.

Figures 1 (a) & (b) contain DGMs for the case where the state variable is directly observable, i.e., the observation model  $\mathcal{H}$  is the unitary operator. In our case, these models correspond to the case of on-site inspections. In Figure 1 (a), we are interested in learning CITL directly at a given moment in time. Thus the state model  $\mathcal{F}$  becomes a probability density function (pdf) with known parameters  $\theta$ . On the other hand, in the DGM of Figure 1 (b), we are interested in inferring the parameters of the deterioration model to make decisions at the lifecycle level.

The DGMs in Figures 1 (c) & (d) refer to cases where the state variable is not directly observable, as in the case of strain-based SHM. In these cases, the observation model is typically a model describing the structural response, parametrised with respect to thickness loss, e.g., a FE model or a data-driven surrogate of that model. Figure 1 (c) corresponds to the case where we're interested at a given moment in time—thus, the state model becomes a prior for CITL—whereas in Figure 1 (d) the goal is to use inference results at the lifecycle level. In all cases described by the DGMs in Figure 1, the observation noise term  $\xi$  is also inferred from data. The probabilistic model employed to describe this term and the resulting inferential QoI are elaborated in the discussion surrounding Eqs. (3) & (4).

The final DGM contains the general BMU problem, from which all other cases can be derived under the specific conditions that were described previously. Therefore, it will be used from this point onward as the reference problem for which all definitions will be given. Some further elaboration is required first. Namely, since all investigations take place in a numerical setting, where the choice of deterioration model rests on the analyst, we will not consider the process noise term  $\psi$ . Moreover, we assume that the observation model operator  $\mathcal{H}$  is deterministic, which means that  $\Phi$  will also be dropped going forward. In this setting, the problem QoIs are collected in the random vector  $\boldsymbol{\theta} \in \mathbb{R}^{d_\theta}$ . Using Bayes' theorem, we can obtain the posterior distribution over the parameters  $\boldsymbol{\theta}$  given a set of observations  $\mathbf{y}$ , as follows:

$$p(\boldsymbol{\theta}|\mathbf{y}) = \frac{p(\mathbf{y}|\boldsymbol{\theta})p(\boldsymbol{\theta})}{\int_{\mathcal{D}_\theta} p(\mathbf{y}|\boldsymbol{\theta})p(\boldsymbol{\theta}) d\boldsymbol{\theta}} \quad (3)$$

where  $p(\mathbf{y}|\boldsymbol{\theta})$  denotes the likelihood function,  $p(\boldsymbol{\theta})$  is the prior over the QoIs and the integral in the denominator is the Bayesian evidence term. The choice of prior may be either empirical or subjective, but ultimately, rests on the analyst.

For the class of problems we are concerned with, constructing the likelihood function relies on assuming a probabilistic model for the observation noise term  $\boldsymbol{\xi}$  in Eq. (1). This is commonly referred to as the prediction error model [36], since it describes the statistical structure between observations and observation model predictions. Here, we will follow the common assumption that the prediction error follows a zero-mean, spherical Gaussian distribution, i.e.,  $\boldsymbol{\xi} \sim \mathcal{N}(\mathbf{0}, \sigma^2 \cdot \mathbf{I}_N)$ , where  $\mathbf{I}_N$  is the  $N$ -dimensional identity matrix and  $\sigma$  is the (scalar) standard deviation, which we will also attempt to learn from the data. Ultimately, we can write the likelihood function as:

$$p(\mathbf{y}|\boldsymbol{\theta}) = \prod_{k=1}^K \prod_{i=1}^N \mathcal{N}(\mathbf{y}_{i,k} - \hat{\mathbf{y}}_{i,k}; 0, \sigma^2) \quad (4)$$

where  $\hat{\mathbf{y}}_{i,k} = \mathcal{H}(\mathcal{F}(t_k; \boldsymbol{\theta}))$  and stochastic independence has also been assumed for the observations at different points in time. For the problems considered in this work, and in most practical applications, the likelihood and prior in the numerator of Eq. (3) do not form a conjugate pair. This means that the evidence term is intractable and no analytical expression for the posterior is available. Therefore, throughout this work we will employ sampling methods, namely Markov Chain Monte Carlo (MCMC), that approximate the true posterior distribution by drawing samples from it. Details about the particular algorithms that have been used will be elaborated on in later sections focused on implementation.

## 2.2. Defining the value of information

The VoI is the product of a Bayesian decision analysis, where the notions of the prior and posterior distributions play a key role. To define the VoI, we first need to consider the decision-making framework underpinning the maintenance planning of deteriorating structural systems. The key quantity in the decision analysis is the state vector  $\boldsymbol{\theta}$ , which quantifies the decision-maker's understanding of the level of deterioration experienced by the structure in question. Quantifying the VoI boils down to assessing whether a given investment in acquiring more information about the structure will improve this understanding, so that substantially better decisions can be made for the O&M of the structure.

The first step in this process is known as a *prior decision analysis*, and is quite similar to traditional engineering practice. In this setting, the decision-maker has no way of acquiring information about the current state of the structure; therefore, maintenance decisions have to take place using only prior information. This information can be based on historical data, i.e., past records of the operation of similar structures, or on the judgement of the decision-maker. Inevitably, the optimal maintenance decision will be the one incurring the lowest loss, which at a given moment in time  $t_k$  of the lifetime of the structure, can be expressed as:

$$d_{\text{prior}}^{(k)} = \arg \min_{d_j} \mathcal{C}_{\text{prior}}^{(k)}(d_j) \quad (5)$$

Where  $d_j \in \mathbf{d} = \{d_0, \dots, d_D\}$  belongs to a discrete set of  $D$  possible maintenance decisions and  $\mathcal{C}_{\text{prior}}^{(k)}$  refers to the prior expected loss or Bayes risk at time  $t_k$  of the life of the structure, which in turn can be defined as:

$$\mathcal{C}_{\text{prior}}^{(k)}(d_j) = \mathbb{E}_{p(\boldsymbol{\theta})} [\mathcal{R}(d_j, \boldsymbol{\theta}) \cdot (1 + r_k)^{t_k}] \quad (6)$$

Where  $\mathbb{E}_{p(\boldsymbol{\theta})}$  is the expected value operator with respect to the prior distribution and  $\mathcal{R}(d_j, \boldsymbol{\theta})$  refers to the consequence cost of making decision  $d_j$ . It should be noted that the consequence cost function is expressed here in general terms. In the following sections, we provide the explicit definition used in this work and discuss its connection to the state variable. The term multiplying the consequence cost represents an inflation adjustment to define the cost at any future time  $t_k$ , when a decision is made. The inflation adjustment is based on the yearly inflation rate  $r_k$  and is aligned with the formulation found in Chadha et al. [30], which introduced the definition of the VoI employed in this work.

The inflation rate has been chosen instead of a discount rate, since it offers a straightforward and consistent way to represent cost trends. This makes it particularly suitable when concrete data about actual costs are unavailable, as is the case in this work. In contrast, defining a discount rate without such data requires making subjective assumptions about quantities such as opportunity cost or the time value of money, which—if not made carefully—could jeopardise the interpretability of results. A similar trend can be observed in the literature, where works defining costs in a normalised (unit-less) manner tend to employ inflation adjustments, e.g., [30–32], whereas those that consider concrete (dollar) costs employ a discount rate, e.g., [21, 28]. Ultimately, the prior expected loss over the entire lifecycle of the structure can be expressed as:

$$\mathcal{C}_{\text{prior}} = \sum_{k=1}^K \mathcal{C}_{\text{prior}}^{(k)}(d_{\text{prior}}^{(k)}) \quad (7)$$

The next step in the process to quantify the VoI is the *pre-posterior decision analysis*, which is fundamental for a VoI-based assessment of an under-design SHM system. The reason is that a *posterior decision analysis*—the immediate extension to the prior—cannot be performed during the SHM system design process, simply because SHM data is not expected to be available *before* the system is installed. Therefore, to perform a pre-posterior decision analysis, synthetic data have to be generated that correspond to potential outcomes of the monitoring system. In the context of SHM system design, it is reasonable to consider multiple candidate monitoring strategies, which we denote here as  $\mathbf{z} = \{z_1, \dots, z_{d_z}\}$ , where  $d_z$  denotes the number of candidates. Accordingly, we will index the observation vectors according to each monitoring strategy, i.e.,  $\mathbf{y}_{z_i}$ . The observation

vector is also considered as random to model uncertainty associated with data collection. As with the prior decision analysis, the optimal decision at any given point in time  $t_k$  for the *pre-posterior* decision analysis is that which satisfies:

$$d_{\text{pre}}^{(k)}(z_i) = \arg \min_{d_i} \mathcal{C}_{\text{pre}}^{(k)}(d_j; \mathbf{y}_{z_i}) \quad (8)$$

Where  $\mathcal{C}_{\text{pre}}^{(k)}(d_j; \mathbf{y}_{z_i})$  represents the conditional expected loss or Bayes risk for a specific decision outcome  $d_j$  and a specific set of observations obtained from a specific monitoring strategy,  $\mathbf{y}_{z_i}$ . Analogous to Eq. (6), the conditional expected loss expands to:

$$\mathcal{C}_{\text{pre}}^{(k)}(d_j; \mathbf{y}_{z_i}) = \mathbb{E}_{p(\boldsymbol{\theta}|\mathbf{y}_{z_i})} [\mathcal{R}(d_j, \boldsymbol{\theta}) \cdot (1 + r_k)^{t_k}] \quad (9)$$

Eq. (9) represents an intermediate step in the *pre-posterior* decision analysis, since it accounts for the updated knowledge obtained for a specific realisation of the monitoring data; consequently, the expectation is taken with respect to the posterior distribution of the state variable  $p(\boldsymbol{\theta}|\mathbf{y}_{z_i})$  for a specific outcome of a specific monitoring strategy ( $\mathbf{y}_{z_i}$ ).

To estimate the expected loss or Bayes risk over the entire lifecycle, we must also account for uncertainty in the outcomes of the information acquisition strategy. Thus, using the optimal decision of Eq. (8), we can obtain the expected *pre-posterior* loss as the expected value of Eq. (9) with respect to the pdf of the observation vectors corresponding to different monitoring strategies. This reads:

$$\mathcal{C}_{\text{pre}}^{(k)}(z_i) = \mathbb{E}_{p(\mathbf{y}_{z_i})} [\mathcal{C}_{\text{pre}}^{(k)}(d_{\text{pre}}^{(k)}(z_i); \mathbf{y}_{z_i})] \quad (10)$$

Obtaining the expected *pre-posterior* loss over the lifecycle of the structure for a particular monitoring strategy requires considering the installation and O&M costs for the monitoring system. Assuming the O&M costs compound annually and the installation cost is paid at the present time, the expected lifecycle pre-posterior loss for a particular monitoring strategy can be defined as:

$$\mathcal{C}_{\text{pre}}(z_i) = \underbrace{\mathcal{C}(z_i) + \sum_{m=1}^M \mathcal{C}_{\text{O\&M}}^{(m)}(z_i) \cdot (1 + r_m)^{t_m}}_{\text{intrinsic}} + \underbrace{\sum_{k=1}^K \mathcal{C}_{\text{pre}}^{(k)}(z_i)}_{\text{extrinsic}} \quad (11)$$

where  $M$  refers to the number of years of operation for which the system is designed. The total cost consists of intrinsic (system-related) costs, i.e., installation and O&M, and the extrinsic decision-making cost. The expected value of information (EVOI) is intuitively defined as the difference between the expected loss estimated using the prior decision analysis and that using the pre-posterior. Namely:

$$\begin{aligned} \text{EVOI}(z_i) &= \mathcal{C}_{\text{prior}} - \mathcal{C}_{\text{pre}}(z_i) \\ &= \mathcal{C}_{\text{S}}(z_i) - (\mathcal{C}(z_i) + \mathcal{C}_{\text{O\&M}}(z_i)) \end{aligned} \quad (12)$$

where  $\mathcal{C}_{\text{O\&M}}(z_i)$  refers to total O&M cost and we have also introduced the notion of the expected



cost savings  $\mathcal{C}_S(z_i)$  [30] defined as:

$$\begin{aligned} \mathcal{C}_S(z_i) = & \sum_{k=1}^K \left\{ \mathbb{E}_{p(\theta)} \left[ \mathcal{R} \left( d_{\text{prior}}^{(k)}, \theta \right) \cdot (1 + r_k)^{t_k} \right] \right\} \\ & - \sum_{k=1}^K \left\{ \mathbb{E}_{p(y_{z_i})} \left[ \mathbb{E}_{p(\theta|y_{z_i})} \left[ \mathcal{R} \left( d_{\text{pre}}^{(k)}(z_i), \theta \right) \cdot (1 + r_k)^{t_k} \right] \right] \right\} \end{aligned} \quad (13)$$

Essentially, Eq. (13) quantifies the value added by acquiring monitoring information to make maintenance-related decisions. For an SHM system design to be feasible in the first place this quantity must be strictly positive; furthermore, it must be greater than the intrinsic costs of the system to justify investment. Therefore, feasible SHM designs are characterised by a positive EVOI. Here, we will not use this (classic) definition, but rather the alternative proposed by Chadha et al. [30], which is known as the expected reward to investment risk ratio, and is defined as:

$$\lambda(z_i) = \frac{\mathcal{C}_S(z_i)}{\mathcal{C}(z_i) + \mathcal{C}_{\text{O\&M}}(z_i)} \quad (14)$$

where now feasible designs are those for which  $\lambda(z_i) > 1$ . By effectively normalising out the monetary units, this definition adds a more qualitative dimension and is arguably better suited to this work, which lacks information about actual cost values. Finally, to compare different information acquisition strategies—not strictly SHM—we can use the relative risk-adjusted reward, which is defined as follows:

$$\chi(z_1, z_2) = \frac{\lambda(z_2) - 1}{\lambda(z_1) - 1} \quad (15)$$

It is interesting to note here that if we apply this metric to compare a candidate SHM strategy to a monitoring strategy consisting solely of inspections, we can obtain—at least qualitatively—a similar metric to the Value of SHM proposed by Kamariotis et al. [28].

### 2.3. Defining a decision setting for CITL monitoring

The expected costs in Eqs. (6), (9), & (10) follow the definition provided by Chadha et al. [30], where the relevant consequence cost functions were defined using the state variable directly. In this work, we will deviate from this approach and use a derivative quantity, which still requires the pdf, or a sample, of the state variable to be defined. More specifically, we will use an exceedance probability estimate, defined for a particular threshold value of the state variable, i.e, CITL. In our view, this provides a more informative attribute, from the perspective of the decision-maker, on which to define consequence costs for maintenance-related decisions. The reason is that, in practice, decision-makers tend to place greater importance on threshold values or acceptable limits, as opposed to direct estimates of some QoI. Furthermore, this definition implicitly enables modelling the risk perception of a decision-maker, through the choice of threshold value.

Let us consider that a sample of CITL realisations  $\{\Delta\tau_n(t_k)\}_{n=1}^{N_{\text{CITL}}}$  is available at time  $t_k$ . These realisations may have been obtained from either a prior or a posterior distribution; it is possible that they were obtained directly or through forward uncertainty propagation of the state model parameters according to Eq. (1). In any case, let us also define an RV to describe the threshold value, namely  $\Delta\mathcal{T}^{(\text{th})} : \Omega_{\Delta\mathcal{T}^{(\text{th})}} \rightarrow \mathbb{R}$ , which is described by its pdf  $p(\Delta\tau^{(\text{th})})$ . We treat this quantity

as a random variable in order to model the epistemic uncertainty inherent in our assumption that CITL is uniform—which in reality is rarely the case.

The pdf  $p(\Delta\tau^{(\text{th})})$  must be chosen appropriately to reflect the epistemic uncertainty modelling assumption. Therefore, its shape must be such that no unnecessary bias is added to the analysis, e.g., one should avoid heavy-tailed distributions. Additionally, its parameters should be selected such that its support corresponds to physically meaningful values, in terms of the CITL threshold. This can be achieved either explicitly by the choice of probability model, or implicitly through sampling considerations.

We can define the *interval* exceedance probability at time  $t_k$  as:

$$\hat{P}_{\text{ex}}^{(i)}(t_k) = \mathbb{P}[\Delta\mathcal{T}(t_k) > \Delta\mathcal{T}^{(\text{th})}] \approx \frac{1}{N_{\text{CITL}}} \sum_{n=1}^{N_{\text{CITL}}} \mathbb{I}[\Delta\tau_n(t_k) > \Delta\tau_n^{(\text{th})}] \quad (16)$$

where  $\mathbb{I}[\cdot]$  is the indicator function and  $\Delta\tau_n^{(\text{th})}$  is a realisation drawn from  $\Delta\mathcal{T}^{(\text{th})}$ . The estimator defined by Eq. (16) is a typical Monte Carlo (MC) estimator, and thus the number of posterior samples  $N_{\text{CITL}}$  has to be chosen so that the estimated probabilities converge to their true values. Further discussion on the convergence characteristics of this estimator will be given in later sections.

$\hat{P}_{\text{ex}}^{(i)}(t_k)$  expresses the probability that CITL levels at a given point in time have exceeded a particular threshold value. By definition, it does not account for potential exceedance events happening prior to time  $t_k$ . Therefore, we will use a cumulative exceedance probability as the attribute on which to define our consequence functions. This probability, denoted as  $p_{\text{ex}}^{(k)}$ , is defined as the complement of the probability of non-exceedance up to time  $t_k$ , assuming that non-exceedance events are independent. It reads:

$$p_{\text{ex}}^{(k)} = \hat{P}_{\text{ex}}^{(c)}(t_k) = 1 - \prod_{j=1}^k [1 - \hat{P}_{\text{ex}}^{(i)}(t_j)] \quad (17)$$

#### 2.4. Defining consequence cost functions

To define the consequence cost functions, we must first decide on an action/decision setting, i.e., we must determine the characteristics of the decision set  $\mathbf{d}$ . Here, we employ a simple binary decision setting, i.e.,  $\mathbf{d} = \{d_0, d_1\}$ , where  $d_0$  refers to the decision not to repair, while  $d_1$  refers to the decision to repair. Accordingly, we shall define a consequence cost function for each decision, parametrised with respect to the cumulative exceedance probability. In this work, we chose to employ linear consequence cost functions, and therefore, in principle, a risk-neutral approach. The cost functions are illustrated indicatively in Figure 2.

Consequence costs have been defined in a normalised manner, i.e., between 0 and 1, due to a lack of available information related to the case study employed in this work. We have chosen this normalised definition because it enables cost extrema to be defined rationally and also allows for a straightforward interpretation of the relative relationship between different costs. Accordingly, the maximum overall cost is set to 1 and corresponds to the case where the decision has been made not to repair, while the cumulative exceedance probability with respect to a particular CITL threshold tends to 1. Conversely, the minimum cost value is set to 0 and is assigned to the case when the decision not to repair has been made, but this time  $p_{\text{ex}}^{(k)} \rightarrow 0$ . Therefore, the corresponding

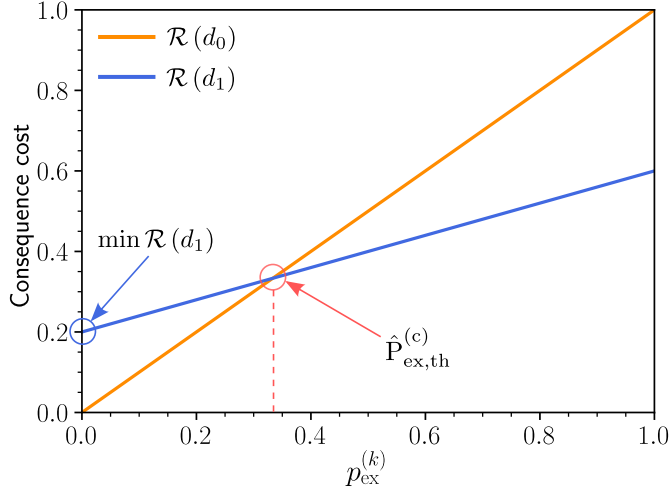


Figure 2: Consequence cost functions for  $\mathbf{d} = \{d_0, d_1\}$ .

consequence cost function is simply defined as:

$$\mathcal{R}(d_0, p_{\text{ex}}^{(k)}) = p_{\text{ex}}^{(k)} \quad (18)$$

The consequence cost function for the decision to repair, i.e.,  $d_1$ , is defined using two parameters that can be interpreted as indicators of the risk profile of the decision-maker. The first of these, denoted as  $\min \mathcal{R}(d_1)$ , is the cost to assign a repair to a structure when the probability of exceeding the maintenance-related threshold is near-zero. This is equivalent to the false alarm cost, and can be interpreted as indicative of the risk-averse, or risk-seeking, tendencies of a decision-maker.

The second parameter is a threshold value of the exceedance probability, denoted as  $\hat{P}_{\text{ex,th}}^{(c)}$ , above which the decision-maker always prefers to conduct repairs. Therefore, this parameter also serves as a means to implicitly model the risk perception of the decision-maker. According to its definition, this parameter corresponds to the intersection point of the two functions, which leads to the following definition for the decision-to-repair consequence cost:

$$\mathcal{R}(d_1, p_{\text{ex}}^{(k)}) = \min \mathcal{L}(d_1) + \left[ 1 - \frac{\min \mathcal{R}(d_1)}{\hat{P}_{\text{ex,th}}^{(c)}} \right] \cdot p_{\text{ex}}^{(k)} \quad (19)$$

At this point, it is important to acknowledge that, while the consequence cost functions we defined earlier can be interpreted as including a level of risk perception modelling, they do not constitute formal utility functions from a decision-theoretic point of view. Therefore, they can be viewed as occupying a middle ground between a risk-neutral approach and the comprehensive treatment presented in Chadha et al. [31].

## 2.5. Computational implementation

In previous sections, the expected loss or Bayes risk was defined in a formal manner; at this point, we will discuss how to computationally implement the VoI calculation framework. Algorithm 1 contains a step-by-step description of the implementation process. We noted earlier that sampling

methods will be used to obtain the posterior distribution for all BMU problems considered here. Inevitably, sampling methods will also be used to compute the various expected values required to calculate the VoI. We will use crude MC estimators, similar to Eq. (16); we have not included them explicitly in the formulation to avoid making the notation too dense. More information, in terms of sample size etc., will be given in later sections discussing the implementation and results of the framework.

---

**Algorithm 1:** Computational implementation for VoI calculation

---

**Input** : Deterioration model  $\mathcal{F}(t; \boldsymbol{\theta})$ , observation model  $\mathcal{H}(t; \boldsymbol{\phi})$ , discrete time points  $t_k$ , decision set  $\mathbf{d}$ , consequence cost functions  $\mathcal{R}(\mathbf{d})$ , candidate monitoring strategies  $\mathbf{z}$ , deterioration model parameter prior  $p(\boldsymbol{\theta})$ , CITL threshold  $\Delta\tau^{(\text{th})} = p(\Delta\tau^{(\text{th})})$ ;

**Output:** EVOI( $z_i$ ),  $\lambda(z_i)$ ,  $\chi(z_i, z_j)$ ;

- 1 **Draw**  $\{\boldsymbol{\theta}_n\}_{n=1}^{n_{\text{prior}}}$  MC samples from  $p(\boldsymbol{\theta})$ ;
- 2 **Set**  $\{\Delta\tau_n(t_k)\}_{n=1}^{n_{\text{prior}}} \leftarrow \mathcal{F}(t_k; \boldsymbol{\theta}_n)$ ;
- 3 **Draw**  $\{\Delta\tau_n^{(\text{th})}\}_{n=1}^{n_{\text{prior}}}$  MC samples from  $p(\Delta\tau^{(\text{th})})$ ;
- 4 *Prior decision analysis*;
- 5 **Compute**  $p_{\text{ex}}^{(k)}$  (Eq. (16) - (17));
- 6 **Compute**  $\mathcal{R}((d_i), p_{\text{ex}}^{(k)})$  (Eq. (18) - (19));
- 7 **Compute**  $\mathcal{C}_{\text{prior}}^{(k)}$  (5) - (6);
- 8 *Pre-Posterior decision analysis*;
- 9 **Set**  $\{\mathbf{y}_{z_i}^{(n)}\}_{n=1}^{n_{\text{prior}}} \leftarrow \mathcal{H}(\Delta\tau_n(t_k))$ ;
- 10 **for**  $n \leftarrow 1$  **to**  $n_{\text{prior}}$  **do**
- 11     **Compute** Posterior sample  $\boldsymbol{\theta}_{\text{pos}}^{(n)} = \{\boldsymbol{\theta}_j \mid \mathbf{y}_{z_i}^{(n)}\}_{j=1}^{n_{\text{pos}}}$ ;
- 12     **Set**  $\{\Delta\tau_n(t_k)\}_{n=1}^{n_{\text{pos}}} \leftarrow \mathcal{F}(t_k; \boldsymbol{\theta}_{\text{pos}}^{(n)})$ ;
- 13     **Compute**  $p_{\text{ex}}^{(k)}$  (Eq. (16) - (17);
- 14     **Compute**  $\mathcal{R}((d_i), p_{\text{ex}}^{(k)})$  (Eq. (18) - (19));
- 15     **Compute**  $\mathcal{C}_{\text{pre}}^{(k)}(d_{\text{pre}}^{(k)}(z_i); \mathbf{y}_{z_i}^{(n)})$  (Eq. (8) - (9));
- 16 **Set**  $\mathcal{C}_{\text{pre}}^{(k)}(z_i) \leftarrow \frac{1}{n_{\text{prior}}} \sum_n \mathcal{C}_{\text{pre}}^{(k)}(d_{\text{pre}}^{(k)}(z_i); \mathbf{y}_{z_i}^{(n)})$  (Eq. (10));
- 17 **Compute**  $\mathcal{C}_{\text{prior}}$  &  $\mathcal{C}_{\text{pre}}(z_i)$  ((7) - (11));
- 18 **Compute** EVOI( $z_i$ ),  $\lambda(z_i)$ ,  $\chi(z_i, z_j)$  ((12) - (15) ;

---

### 3. Case study description

This section contains a description of the various aspects of the case study used to demonstrate the framework presented in this work. It includes defining the stochastic deterioration model, as well as the different monitoring strategies and their associated observation models.

#### 3.1. Probabilistic CITL modelling

Performing a pre-posterior decision analysis requires generating realisations of the deterioration process. These realisations represent potential deterioration histories that the structure is expected to experience during its lifecycle. In this work, we assume that the deterioration model has a known parametric structure characterised by the parameter vector  $\boldsymbol{\theta}$ . More specifically, we will use the following expression to describe CITL evolution:

$$\Delta\tau_k = \mathcal{F}(t_k; \boldsymbol{\theta}) = \frac{\gamma}{\alpha + \beta \exp(-(t_k - t_0))} \quad (20)$$

where  $\boldsymbol{\theta} = \{\alpha, \beta, \gamma\}$  and  $t_0$  refers to the time of corrosion initiation, which is considered to be known and is assumed here to be the 10<sup>th</sup> year of vessel operation. The logistic-type model of Eq. (20) is similar to the model proposed by Qin et al. [10], although here the term in the numerator is learnt from data, whereas in the original it represents the (known) maximum observed CITL level. This choice of model leads to CITL realisations that are consistent with historically observed data and the commonly understood physics of corrosion evolution. Namely, this model exhibits asymptotic behaviour, which is expected in plate-like components subjected to uniform corrosion, since corrosion by-products accumulate on their surface leading to a deceleration of the phenomenon.

According to steps 2-4 of Algorithm 1, to generate realisations from the CITL prior process, we must first define the joint prior distribution over the deterioration model parameters  $p(\boldsymbol{\theta})$ . We will assume that the model parameters are independent RVs, and select their priors so that the resulting CITL prior process is physically consistent. More specifically, we assume the following parameter priors:

$$\begin{aligned} \alpha &\sim \mathcal{U}(4., 13.) \\ \beta &\sim \mathcal{N}(250., 50.) \\ \gamma &\sim \mathcal{U}(4., 8.5) \end{aligned} \quad (21)$$

To explain the choice of these priors, let us consider the CITL prior process realisations depicted in Figure 3. These have been generated by first drawing  $n_{\text{prior}} = 1000$  samples independently from each distribution of Eq. (21) and then propagating them through the deterioration model (Step 4, Algorithm 1). An 8-year period—starting from  $t_0 = 10$  years—has been assumed, where corrosion is active and simultaneously being monitored. Our choice of priors, alongside the model structure, ensures that the resulting CITL realisations satisfy several physical constraints. First, it leads to strictly positive, monotonically increasing CITL realisations. Moreover, it ensures that maximum CITL levels remain within acceptable limits consistent with practical experience, i.e., they are below 20% of the as-built plate thickness. This is a threshold level for which regulators typically prescribe plate renewal; thus, our choice of priors leads to realistic scenarios. Finally, these parameter priors lead to a relatively wide prior process which is desirable from a mathematical standpoint, since it ensures that (unnecessary) biases are not included in the model.

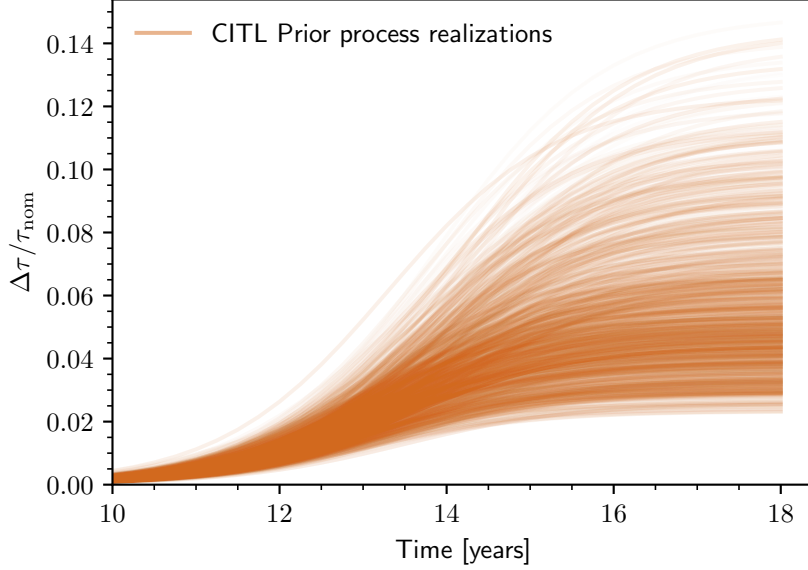


Figure 3: CITL prior process realisations expressed as a fraction of the as-built plate thickness  $\tau_{\text{nom}} = 14$  mm.

### 3.2. Defining monitoring strategies

The generated CITL realisations will be used to obtain corresponding realisations of the observation vectors of the different monitoring strategies for which we seek to quantify the VoI. These observation vector realisations can then be used to quantify the uncertainty associated with acquiring information through the MC estimator of the expectation in Eq. (10)—in computational terms, Steps 18 & 20 of Algorithm 1. The first step in this process is to define the different monitoring strategies that are of interest in this work. We will consider the following:

- *Inspection only* ( $z_0$ ): A single inspection event takes place at  $t_{\text{insp}} = 15$  years. CITL is directly observable.
- *Strain-based CITL identification* ( $z_1$ ): Strain data is used to identify the level of CITL directly at different points in time.
- *Strain-based CITL monitoring (limited data)* ( $z_2$ ): Strain data is used to infer the parameters of a CITL deterioration model. A limited number of observations is considered.
- *Strain-based CITL monitoring* ( $z_3$ ): The same scenario as  $z_2$  with more available observations.

It is important to explain the rationale behind each candidate monitoring strategy, and how it relates to maintenance planning. The inspection-only strategy provides a basis for comparison with current CITL inspection practices and the inspection time has been chosen to be consistent with a 5-year hull survey. The other three strategies correspond to more typical SHM scenarios, where monitoring takes place more frequently—although not necessarily continuously—and the deterioration process is monitored indirectly, i.e., through its effects on structural response.

Here, we differentiate these SHM scenarios based on two factors: the monitored QoI and the amount of available observations. The former reflects different decision-making biases, e.g., the

decision-maker in  $(z_1)$  does not assume a specific functional form for the deterioration model, compared to all other scenarios. This represents a different attitude towards introducing inductive bias into the model. The second factor reflects different attitudes towards investing in the intrinsic cost of the system, in the sense that acquiring and storing larger quantities of data represents a greater willingness to invest more capital.

### 3.3. Defining observation models

An additional (technical) factor differentiates the candidate monitoring strategies; they require different observation models to generate observation vector realisations, as well as to construct the Bayesian likelihood function of Eq. (4). In the inspection-only case where CITL is directly observable, we consider a probabilistic model (a pdf) as the observation model  $\mathcal{H}$ . For the strain-based SHM scenarios however, we require a structural model that maps CITL to strain at specific locations of interest.

The structural system we employ as the case study to demonstrate the proposed framework is part of a ship hull structure. More specifically, it consists of the three central holds of a product carrier vessel with length  $L_{B.P.} = 174.0$  m, beam  $B = 32.2$  m and depth  $D = 19.1$  m. A perspective view of the (meshed) FE model of this structure is shown in Figure 4 (a), while a zoomed-in view of the region of monitoring interest is shown in Figure 4 (d). This region is located on the inner bottom of Cargo Hold No. 4 (C.H. 4), i.e., the central of the three holds—depicted in more detail in Figure 4 (c). This is the region for which we seek to infer the level of uniform thickness loss, according to the four monitoring strategies described previously.

The level of CITL is considered to be constant, percentage-wise, for all structural components in the green-coloured region of Figure 4 (b), which includes the region of monitoring interest. The green-coloured region corresponds to the water ballast tank in the double bottom of the vessel—depicted using one symmetric half of the hold. Since conditions are relatively similar in the ballast tank, we have assumed a constant corrosion rate, and therefore CITL level, for the corresponding region. Similarly, the regions with different colours in Figure 4 (b) correspond to the other ballast tanks in the cargo hold. Each has been considered to experience a constant level of CITL, which is different to the one in the double bottom. Although not treated directly as inferential QoIs, these CITL levels still affect the structural response as latent variables.

From a monitoring perspective, strategy  $(z_0)$  is unaffected by these latent parameters, since observations are gathered directly from the region of interest. The probabilistic model used to generate these observations can be interpreted as accounting for both measurement uncertainty, as well as spatial variability. However, we must note here that more expressive methods exist to model the latter, e.g., treating CITL as a random field [37], which were considered out of the scope of this paper. We have used the following probabilistic model to generate inspection data:

$$\mathbf{y}_{\text{insp}} \sim \mathcal{N}\left(\Delta\tau(t_{\text{insp}}; \boldsymbol{\theta}_n), (0.1 \cdot \Delta\tau(t_{\text{insp}}; \boldsymbol{\theta}_n))^2\right) \quad (22)$$

which implies that for every prior realisation  $\boldsymbol{\theta}_n$  the inspection observations are normally distributed with a mean equal to the prior process value at the time of inspection, and a coefficient of variation (CoV) equal to 0.1. Note that the probabilistic model of Eq. (22) refers to a scalar RV, from which we ultimately draw  $N$  samples to create the observation vector  $\mathbf{y}_{\text{insp}} = \left\{y_{\text{insp}}^{(i)}\right\}_{i=1}^N$ .

For the strain-based monitoring strategies, the observation model will be based on the FE model of the three compartments presented in Figure 4. This model has been constructed using 4-node

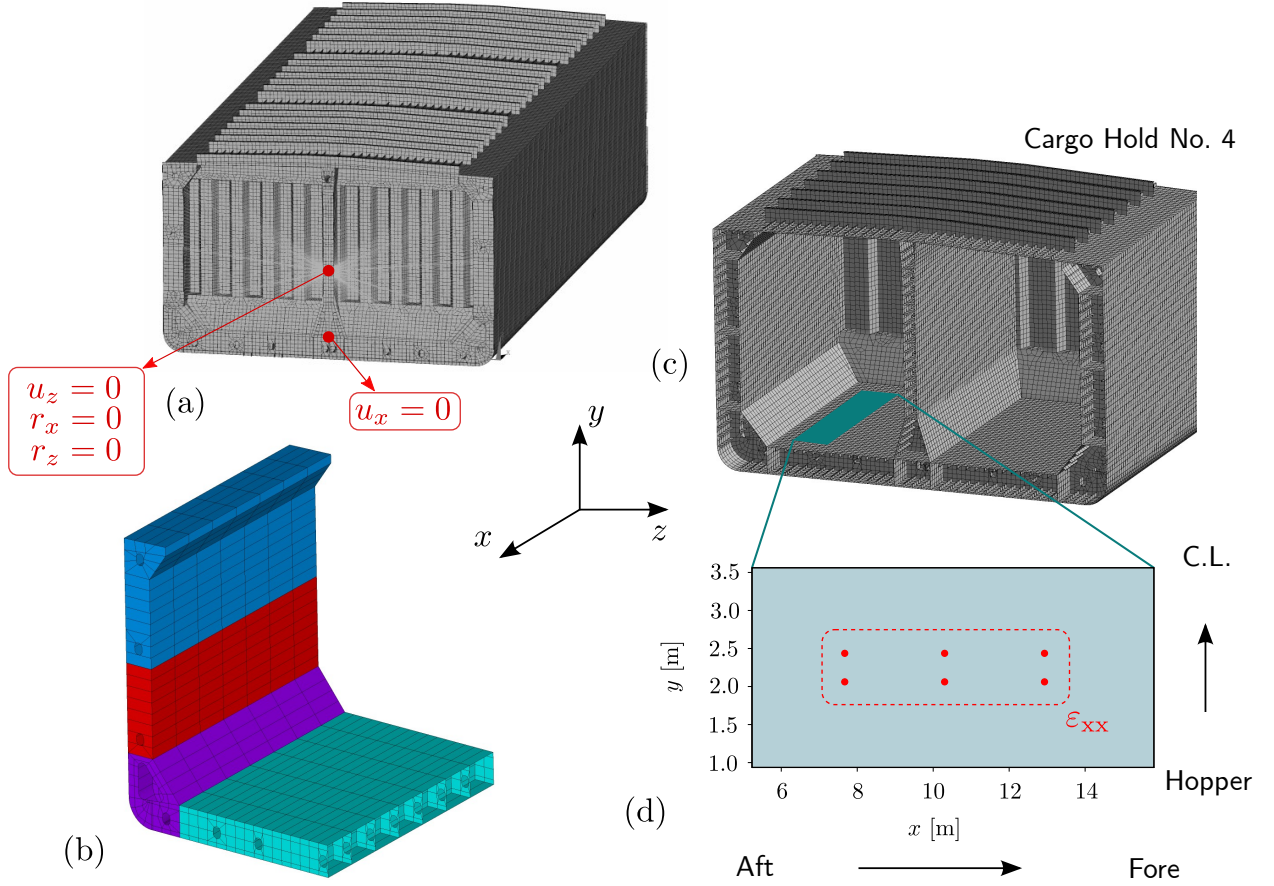


Figure 4: (a) Perspective view of three hold compartment FE model, (b) regions with different CITL levels, (c) interior view OF C.H. 4 & (d) longitudinal strain sensor locations expressed in local coordinates.

linear shell elements for all plate-like structural components and 2-node linear beam elements for all longitudinal stiffeners, as well as flanges attached to primary supporting members, e.g., web frames. An element size of approximately 0.5 m—for a model spanning 63.2 m lengthwise—was employed to generate a generally uniform mesh, excluding areas where further refinement was required, e.g., around the various openings.

Boundary conditions were applied to the model ends using kinematic constraints through master-slave connections. Namely, the degrees of freedom (dof's) shown in Figure 4 (a) were constrained at the master nodes and these constraints were transferred to the slaves using rigid link elements. The slave nodes consist of all nodes attached to longitudinally extending structural members. Longitudinal displacement was constrained on a single node on the longitudinal plane of symmetry of the model to ensure equilibrium. Finally, the model was subjected to external (hydrostatic) and internal (cargo) pressure loads, the latter of which were considered to be stochastic. More specifically, cargo hold filling rates were treated as RVs following the beta distribution, and were defined for a specific loading condition. More details on the applied loads and FE modelling can be found in Sillionis et al. [17] and have not been included here for the sake of brevity.

At this point, it is important to note that the FE model used to generate strain observations has not been validated compared to actual strain measurements, as these are not available for the



reference vessel. A degree of validation has taken place by comparing FE results to analytical or semi-analytical tools used for strength assessment of ship hulls, as reported in [17]. The lack of validation compared to real-world data entails that a level of model form bias is introduced to the analysis. However, the nascent stage of adoption of SHM in ship hulls makes such an assumption largely inevitable.

What is more important in the context of this work is the placement of potential strain sensors; this is ultimately what will define the observation model. We have decided to use six sensor locations measuring longitudinal strain  $\varepsilon_{xx}$ , arranged in an orthogonal grid, as depicted in Figure 4 (d). The location of these sensors and the measured strain component were selected using expert knowledge. Specifically, they are located at the centre of the plate elements defined between the longitudinal stiffeners and transverse webs that make up a typical stiffened panel. Thus, they exhibit relatively high strain values, which offer robustness against noise, and are more sensitive to the stiffness reduction caused by thickness loss, due to being far from stiffer supporting members. For a more in-depth analysis of this selection, the reader is again referred to the earlier work of the authors [17].

The scatter points in Figure 5 represent longitudinal strain data obtained at these locations for different CITL levels. The strain data were obtained using a forward MC process to propagate load- and deterioration-related uncertainty. The latter refers to the variability in CITL that affects the regions neighbouring the double bottom. The dispersion exhibited by the strain data is a result of these two sources of uncertainty. In total, 1000 data points were generated by solving the FE model non-intrusively for different CITL and load realisations, which required approx. 16 hours of wall time in a workstation equipped with 32 GB of RAM and an Intel® Core™ i7-10750H CPU.

The time required for a single FE model solution does not scale well with the computational requirements of MCMC algorithms where likelihood function evaluations, and corresponding calls to the FE solver to evaluate the observation model, number in the tens of thousands. If one also considers the requirements of a pre-posterior decision analysis, where MCMC is run for each prior realisation as well, the computational cost increases by an additional order of magnitude. Therefore, we must train a surrogate of the FE model to serve the purpose of the observation model  $\mathcal{H}$  for the strain-based monitoring strategies.

In this work, we have adopted a deterministic observation model, although latent variables exist that affect the strain response—the aforementioned load- and deterioration-related uncertainty. Using the mean functions of probabilistic surrogate models is relatively common practice (see e.g. [38, 39]). Employing a fully probabilistic observation model requires a marginalised likelihood function formulation to integrate out nuisance (or latent) variables. For the problem in question, the authors have found that, while this leads to marginal improvements in the quality of the posterior distribution, it also requires  $4\times$  wall time. More details on this investigation can be found in Silionis et al. [40], and are not included here in the interest of brevity.

Ultimately, a classic linear regression model is sufficient to capture the mean trend of the strain data, as shown in Figure 5. Bayesian inference (MCMC) was used to obtain posterior distributions of the linear regression model parameters. Although the full posteriors were not used for this particular analysis, adopting a probabilistic surrogate model allows us to be consistent with the general principles presented earlier, as well as with the framework proposed by the authors in [40].

At this point, we believe it is important to comment on certain characteristics of the strain data. It is evident that similar strain patterns are captured at all sensor locations. This implies a certain redundancy in the available observations, which is justified considering the similarity of the

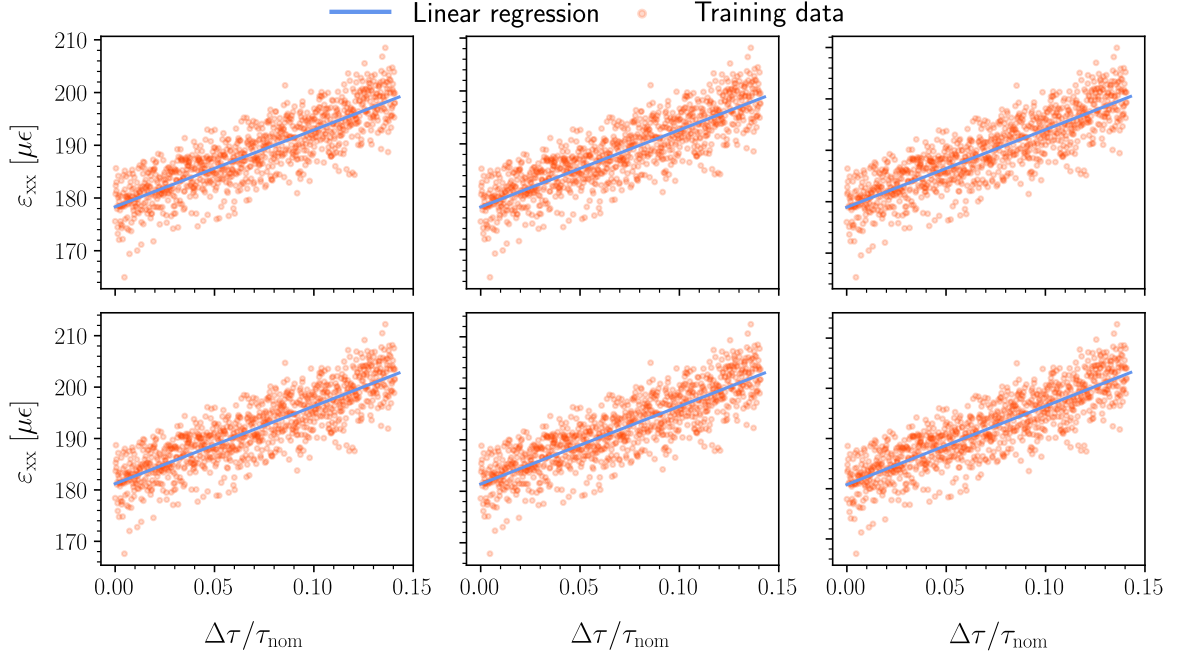


Figure 5: FE-based strain observations at potential sensor locations alongside linear regression-based observation models (figures follow the layout of Figure 4 (d)).

strain features. This in turn, is a result of the similarity in structural arrangement and loading. This redundancy, however, could prove beneficial in mitigating the effects of measurement noise. In the case of higher-dimensional data, feature extraction techniques such as the Singular Value Decomposition could be applied to reduce the feature dimension while preserving their original statistical characteristics.

#### 4. Numerical investigation

This section contains results from the implementation of the proposed VoI quantification framework. First, we present inference results for the BMU problems defined for each monitoring strategy and then discuss the behaviour of the employed limit state function. We investigate the influence of the decision threshold and of different cost assignments on the VoI and, finally, we discuss the relative utility of collecting inspection data.

##### 4.1. Bayesian inference of CITL

The different BMU problems dealt with in the proposed framework can only be solved using sampling methods, the most popular of which is arguably MCMC. MCMC refers to a family of algorithms that draw correlated samples from the target Bayesian posterior by constructing ergodic Markov chains with that posterior as their invariant distribution [41]. Here, we have employed Hamiltonian Monte Carlo (HMC) in the form of the No U-Turn Sampler (NUTS) [42]. NUTS is a variant of HMC that is particularly suited to high-dimensional parameter spaces and exhibits remarkable speed and efficiency in reaching the invariant distribution, i.e., the target posterior. Therefore, it is particularly well-suited to the needs of a pre-posterior decision analysis, where

a large number of MCMC implementations is required, and efficient utilisation of computational resources is critical.

There is a rich literature on HMC in general, and NUTS in particular, e.g., the excellent review of Betancourt [43]. We consider it out of the scope of this paper to provide a detailed description here, so we suggest that the interested reader considers the aforementioned work, as well those referenced earlier [41, 42]. We do note that to implement NUTS we have used the Python probabilistic programming library Numpyro [44, 45], which uses automatic differentiation to calculate the gradients of the Bayesian likelihood function required by NUTS, which for the problem considered here are analytically intractable.

The BMU problem that arises as a result of monitoring strategy ( $z_0$ ) is described by the DGM of Figure 1 (b). Accordingly, our goal here is to infer the deterioration model parameters  $\theta$  using CITL observations directly, alongside the prediction error standard deviation  $\sigma$ . We use the same priors as in Eq. (21) for the former, while for the latter we assume that  $\sigma \sim \text{Half-Normal}(1.0)$ . The choice of a Half-Normal prior ensures that the standard deviation remains strictly positive, while at the same time being relatively uninformative.

The observation model of Eq. (22) is used to generate 50 CITL observations at  $t_{\text{insp}} = 15$  years for each of the 1000 deterioration realisations generated from the prior. For each prior realisation, NUTS is run using 2000 warm-up steps—used to tune algorithm hyperparameters and ensure that the invariant distribution has been reached—and an equal number of draws from the target posterior. Multiple chains starting from different seeds were drawn for randomly selected prior realisations to assess convergence, since it was considered impractical to do this for the entire sample. The rank-normalised  $\hat{R}$  diagnostic was used to quantitatively assess convergence, and was found consistently to be below 1.01, which is the accepted threshold proposed by Vehtari et al. [46]. This procedure was followed for all considered monitoring strategies with similar results.

Figure 6 plots the CITL posterior mean and 95% credible interval (C.I.) against the corresponding target CITL—obtained from the prior process—for several indicative realisations. To obtain

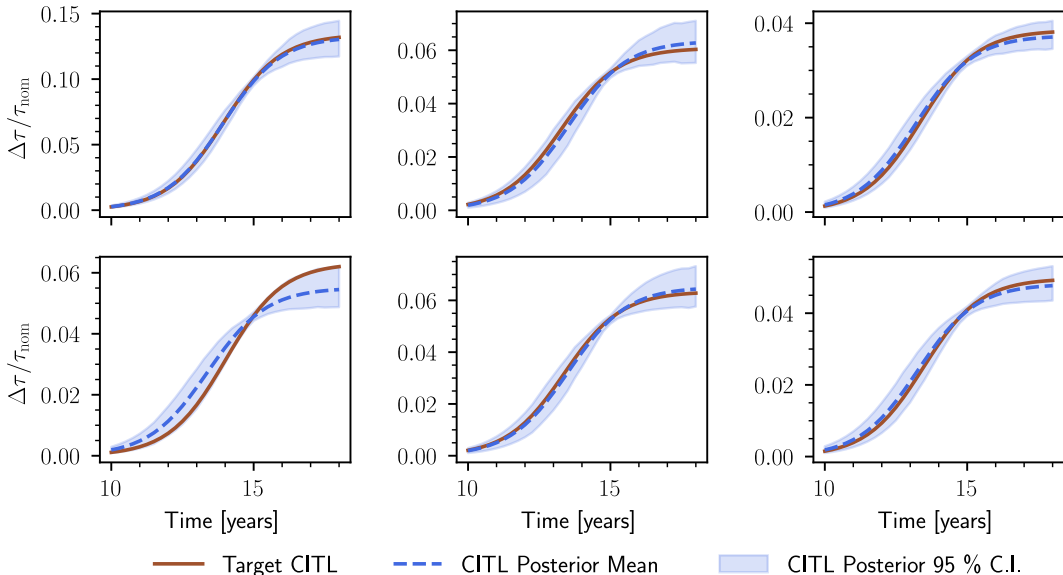


Figure 6: CITL posterior processes for indicative CITL realisations using monitoring strategy ( $z_0$ ).

the CITL posterior process, the samples from the posterior distribution of the deterioration model parameters were propagated through the deterioration model (Eq. (20)). The resulting posterior is able to capture the target deterioration curve fairly accurately, while it is noteworthy that around  $t_{\text{insp}}$  uncertainty is reduced significantly, as evidenced by the narrow C.I. However, it is important to note that the inspection time is crucial for successful inference, with earlier inspections expected to lead to poorer results.

The BMU problem associated with monitoring strategy ( $z_1$ ) is described by the DGM in Figure 1 (c). Here, the QoI is CITL directly, and is inferred at different points in time. We assume a series of independent, identically distributed (i.i.d.) uniform priors for each point, namely  $\Delta\tau \sim \mathcal{U}(0.0, 2.0)$  mm. This choice of prior ensures that CITL is effectively bounded within the range of the prior process realisations, while at the same time ensuring that the surrogate acting as the observation model is not called to make out-of-training predictions.

Strain observations were generated for each prior process realisation at 3-month intervals, with a total of 50 observations generated at each time, using the linear regression-based surrogate. This constitutes a so-called inverse crime, however it is unavoidable due to the nature of the pre-posterior decision analysis. The resulting observations were further corrupted using additive Gaussian noise  $\xi \sim \mathcal{N}(\mathbf{0}, 5 \cdot I_{50}) \mu\epsilon$ , where the standard deviation of  $5 \mu\epsilon$  is representative of the resolution of commonly-used strain sensors [30].

The choice of data acquisition frequency was motivated by the fact that CITL deterioration evolves slowly, as well as by practical considerations related to the observation model. More specifically, to effectively use the static strain-based observation model that is available, the vessel must either be in port or sailing in calm seas. Either of these conditions can be reasonably met by the three-month data acquisition interval.

In terms of implementation, the same hyperparameters were used for NUTS as with ( $z_0$ ). The CITL posterior mean and 95% C.I. are plotted compared to the target CITL values for indicative deterioration realisations in Figure 7. The observed non-smoothness of the posterior process is expected, since no functional form has been assumed for the deterioration model. Here as well,

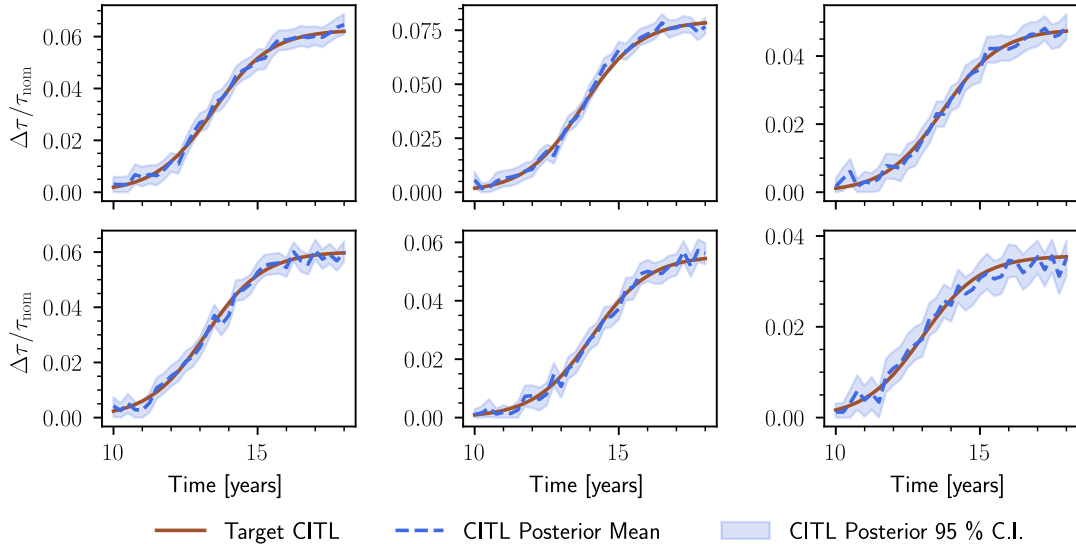


Figure 7: CITL posterior processes for indicative CITL realisations using monitoring strategy ( $z_1$ ).

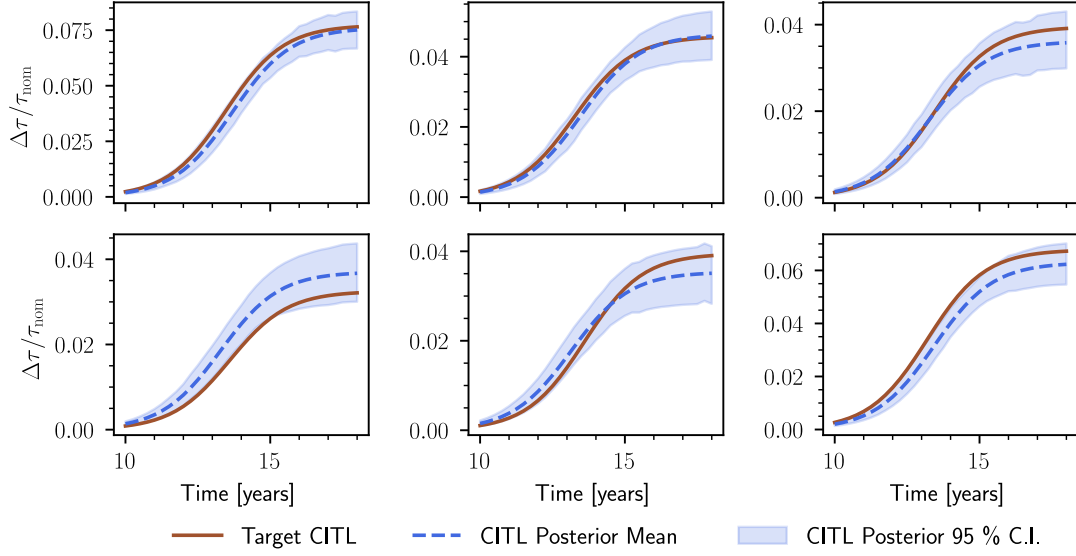


Figure 8: CITL posterior processes for indicative CITL realisations using monitoring strategy ( $z_2$ ).

inference can be judged as fairly successful, although this approach inevitably leads to some violation of the problem physics, as the inferred CITL is not guaranteed to be continuously increasing. The CITL posterior mean at the upper right panel of Figure 7 is a typical example.

Monitoring strategies ( $z_2$ ) & ( $z_3$ ) are associated with the same BMU problem, which is described by the DGM in Figure 1 (d). The deterioration model parameter priors are set according to Eq. (21), while the prediction error standard deviation is again assigned a Half-Normal prior, namely  $\sigma \sim \text{Half-Normal}(1.0)$ . What differentiates the two strategies is the number of strain observations that are considered available at the data acquisition time, which is again set to 3-month intervals. More specifically, a single observation at each point in time is considered for ( $z_2$ ), while 50 are considered for ( $z_3$ ); NUTS is applied using the same hyperparameters as with all previous cases.

Inference results for indicative prior realisations are presented in Figure 8 for ( $z_2$ ) and Figure 9 for ( $z_3$ ). Including more observations has a positive effect, since the CITL posterior for ( $z_3$ ) is characterised by virtually no uncertainty, leading to almost exact predictions of the target. Conversely, inference results in the sparse data regime showcase higher variance; however, the mean function can approximate the target deterioration curve fairly accurately. Crucially, running NUTS for ( $z_2$ ) requires about 1/5 of the computation cost compared to ( $z_3$ ), in terms of wall time.

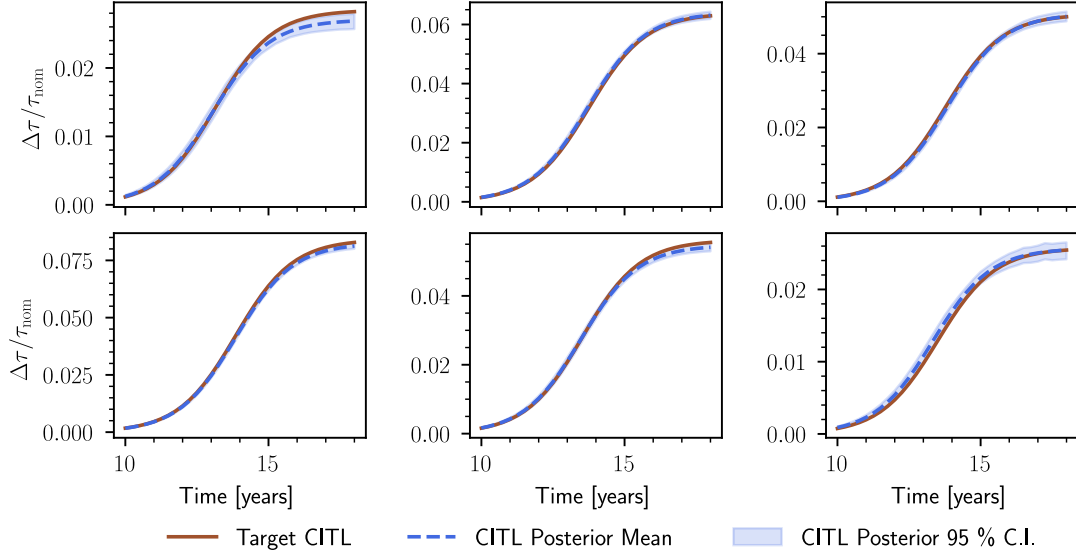


Figure 9: CITL posterior processes for indicative CITL realisations using monitoring strategy ( $z_3$ ).

#### 4.2. Examining the limit state function

At this point, it is important to examine the characteristics of the limit state function, and the corresponding exceedance probability, that we have used to define the consequence cost functions. The computational cost of the pre-posterior decision analysis places significant restrictions on the number of samples that can be drawn from the CITL prior process. This is also true for the samples drawn from the posterior distribution corresponding to each prior process realisation. The number of posterior samples  $n_{\text{post}}$  primarily affects the robustness of the estimator of Eq. (16), while the number of prior samples  $n_{\text{prior}}$  affects the MC estimators of the prior and pre-posterior consequence costs (see Eqs. (6) & (10)). As mentioned earlier, for the purposes of this work we have assumed that  $n_{\text{prior}} = 1000$  and  $n_{\text{post}} = 2000$ .

To gain some insight on the characteristics of the limit state function, let us consider Figure 10 which plots the cumulative exceedance probability  $p_{\text{ex}}^{(k)}$  over the CITL monitoring period. This probability has been calculated using Eq. (17) for both the prior and the pre-posterior decision analysis, assuming a threshold CITL level  $\Delta\tau^{(\text{th})} \sim \mathcal{N}(1.2, (0.05 \cdot 1.2)^2)$  mm. A Gaussian pdf has been assumed since it is symmetric and commonly used to describe statistical discrepancy, thus it does not add any unwanted bias to the epistemic uncertainty modelling represented by the threshold pdf. Additionally, the choice of a 5 % coefficient of variation ensures that threshold realisations remain close to the specified mean value, i.e., the prescribed threshold level. This in turn ensures that no threshold values violating physical constraints, e.g., falling outside the prior range, are generated.

As expected, for the prior decision analysis  $p_{\text{ex}}^{(k)}$  devolves to a single monotonically increasing curve which becomes non-zero after approx. year 14 of vessel operation. At this point in time, CITL deterioration reaches levels nearing the maintenance-related threshold value. This can also be observed by examining the cumulative exceedance probability estimates for the pre-posterior analysis, that correspond to monitoring strategy ( $z_3$ ), but can be considered as indicative of all cases.

The key characteristic of the  $p_{\text{ex}}^{(k)}$  curves in the pre-posterior case is that for a significant number

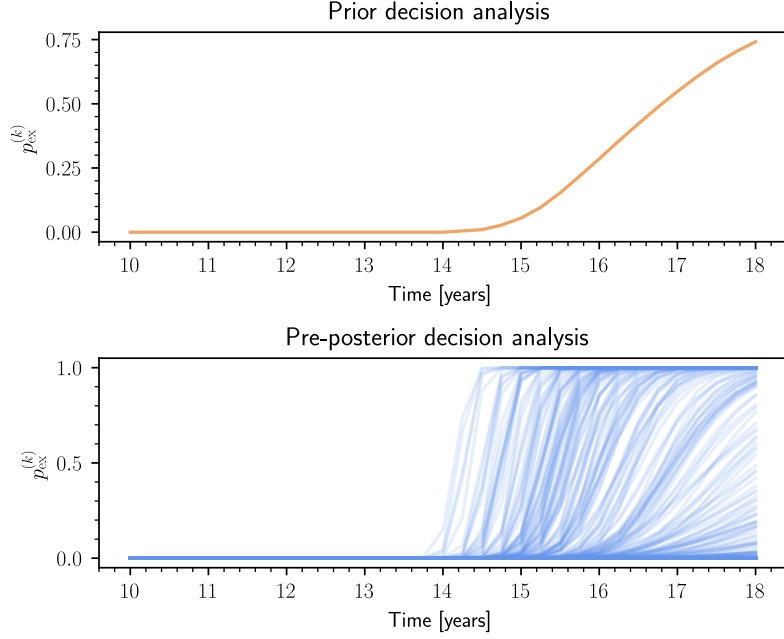


Figure 10: Cumulative exceedance probability over the CITL monitoring period for  $\Delta\tau^{(\text{th})} \sim \mathcal{N}(1.2, (0.05 \cdot 1.2)^2)$  and monitoring strategy ( $z_3$ ).

of deterioration realisations, the exceedance probability rapidly transitions from near-zero to 1. This is indicative of the very narrow CITL posteriors shown in Figure 9. This behaviour causes the exceedance probability estimator to oscillate between 0 and 1, depending on the point in time and the decision threshold. Figure 11 illustrates this behaviour by plotting histograms for the prior CITL realisations at given points in time alongside the corresponding  $p_{\text{ex}}^{(k)}$  histograms obtained via the pre-posterior decision analysis.

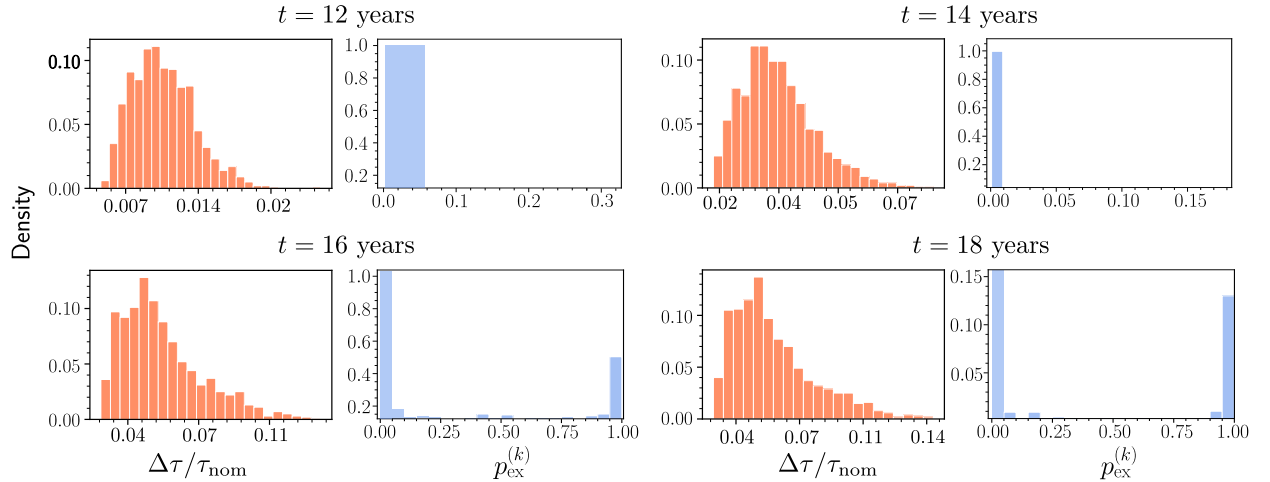


Figure 11: CITL prior realisation histograms (orange) over the CITL monitoring period and corresponding cumulative exceedance probability histograms (blue) from the pre-posterior decision analysis for monitoring strategy ( $z_3$ ).

At points in time where the CITL levels have not reached the threshold, as in the upper panel

of Figure 11, the estimator effectively tends to zero. As time progresses, it is evident from the lower panel of Figure 11 that there is still a proportion of deterioration scenarios for which the threshold has not been exceeded. However, there are relatively few instances where  $p_{\text{ex}}^{(k)}$  attains intermediate values and for the majority of scenarios it tends to 1. This demonstrates that the estimator of Eq. (16) behaves like a discrete variable as a result of the low posterior uncertainty and monotonically increasing nature of the deterioration model. From a practical standpoint, it demonstrates that the employed number of posterior samples does not jeopardise the reliability of the  $p_{\text{ex}}^{(k)}$  estimator.

The high quality of the inference results suggests that the CITL posterior process closely matches the realisations from the prior. We have discussed how the estimator is sufficiently robust for the assumed number of posterior samples. To conclude the discussion in this section, we must now shift our focus on whether the number of prior samples is sufficient. We have adopted an empirical approach to investigate this, which is based on the particular characteristics of our analysis. More specifically, considering the low cost of generating prior realisations, we have drawn  $10^6$  CITL realisations for the assumed monitoring period. By plotting histograms of these realisations at various points in time, we visually determined a suitable pdf to describe them. Using this pdf, we were then able to estimate the interval exceedance probability at different moments in time for different thresholds, again using  $10^6$  samples, to ensure a high level of confidence.

Figure 12 (a) plots an indicative histogram obtained using this procedure for  $t = 16$  years alongside the corresponding log-normal distribution fit. Figure 12 (b) contains a histogram generated by combining all posterior samples obtained during the pre-posterior analysis at the same point in time. These posterior realisations correspond to  $n_{\text{prior}} = 1000$  deterioration scenarios. Their low individual variance (see Fig 9) suggests that they effectively act as copies of the corresponding prior realisation, leading to an exceedance probability estimator that is analogous to a bootstrap estimator. Nevertheless, a log-normal pdf was fit on the posterior realisations as well and exceedance probabilities were estimated for different moments in time and different thresholds.

For a threshold level  $\Delta\tau^{(\text{th})} \sim \mathcal{N}(1.5, (0.05 \cdot 1.5)^2)$  mm at 16 years, the exceedance probability estimated using the prior was approx. 2.21%, while that using the posterior samples approx. 1.94%. This is indicative of the upper tail behaviour of the distributions, where the two estimators are expected to diverge more significantly. At lower threshold levels, the estimators become virtually

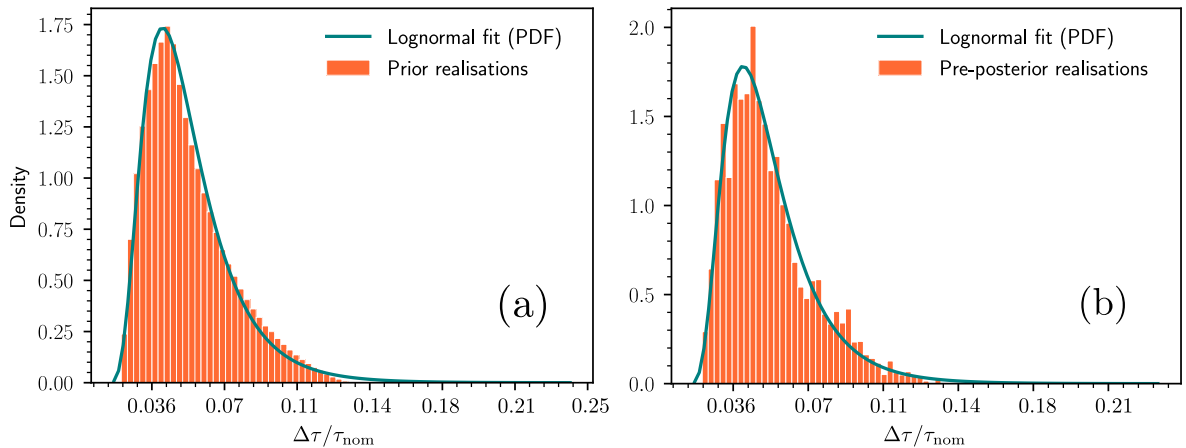


Figure 12: Histograms and fitted log-normal pdfs of (a) CITL prior process realisations and (b) posterior realisations for the entire pre-posterior analysis at  $t = 16$  years.



equivalent. In the context of this work, and considering the definition of the consequence costs (see Figure 2), exceedance probabilities of this order are not expected to affect maintenance decisions, as they are below  $\hat{P}_{\text{ex,th}}^{(c)}$  levels of interest. Therefore, we consider it safe to conclude that the assumed sample sizes are sufficient for our purposes.

#### 4.3. Investigating the effect of the decision threshold

We begin our investigation on the VoI from CITL monitoring by assessing the effect of the decision threshold on the expected reward to investment risk ratio ( $\lambda$ ) of the different strain-based monitoring strategies. To be able to do that, we must first define both the intrinsic and the extrinsic cost associated with each strategy. Due to a lack of specific information about costs, we shall define the intrinsic cost, which includes installation and O&M costs, heuristically.

We assume that monitoring strategy ( $z_2$ ) has the lowest intrinsic costs, and therefore acts as the reference, and define the costs for the other two proportionally. This assumption is based on the fact that it requires the least amount of data between the three strain-based monitoring strategies. Ultimately, we assume that  $\mathcal{C}(z_2) = 0.1 \cdot \mathcal{C}_{\text{max}}$  and  $\mathcal{C}_{\text{O\&M}}(z_2) = 0.01 \cdot \mathcal{C}(z_2)$ , where  $\mathcal{C}_{\text{max}}$  refers to the overall maximum consequence cost, which in this case is equal to 1. We have based these cost assignments—expressed in relative terms—on engineering judgement and the figures reported in Chadha et al. [30].

We then assume that the increased amount of data required by the other two strategies—they use 50 strain observations as opposed to 1 at each data acquisition time—incurs a 10% increase in the installation cost, i.e.,  $\mathcal{C}(z_1) = \mathcal{C}(z_3) = 1.1 \cdot \mathcal{C}(z_2)$ . For the O&M cost, we assume that the increase is proportional to the relative increase in computation cost between the different strategies, therefore  $\mathcal{C}_{\text{O\&M}}(z_1) = 2 \cdot \mathcal{C}_{\text{O\&M}}(z_2)$  and  $\mathcal{C}_{\text{O\&M}}(z_3) = 5 \cdot \mathcal{C}_{\text{O\&M}}(z_2)$ . Finally, we have assumed a constant yearly inflation rate  $r = 2\%$ .

In terms of the extrinsic costs, we have considered two consequence cost definitions—for the decision to repair—denoted as  $\mathcal{R}_1(d_1)$  &  $\mathcal{R}_2(d_1)$ . These consequence costs have been defined for  $(\min \mathcal{R}_1(d_1), \hat{P}_{\text{ex,th}}^{(c)}) = (0.33, 0.2)$  and  $(\min \mathcal{R}_2(d_1), \hat{P}_{\text{ex,th}}^{(c)}) = (0.15, 0.1)$ . According to these definitions, one could interpret  $\mathcal{R}_1(d_1)$  as indicative of a more risk-seeking decision-maker who assigns greater cost to a false call, i.e., an unnecessary repair, and is willing to take more risk in terms of setting a higher maintenance-related CITL threshold. Conversely,  $\mathcal{R}_2(d_1)$  can be interpreted as characterising a more risk-averse individual.

The expected reward to investment risk ratio for the different consequence costs is plotted in Figure 13 for different CITL threshold levels. A similar behaviour is observed for all three strategies, with investment in strain-based monitoring being optimal at intermediate threshold levels. At lower thresholds, the value of acquiring monitoring information is reduced. This can be explained by the behaviour of the prior process at lower CITL values, where realisations are more clustered and exhibit lower variance (see Figure 3). Conversely, at higher thresholds the benefit of investing in monitoring becomes marginal, as  $p_{\text{ex}}^{(k)} \rightarrow 1$  for a large proportion of deterioration scenarios, leading to a significant increase in the compounded repair costs.

Comparing the different monitoring strategies, we observe that ( $z_2$ ), i.e., the reference case, appears to be the optimal. This is a result of the accuracy and low uncertainty of the CITL posteriors, which means that the initial cost assignment is what essentially differentiates the monitoring strategies. Therefore, a more thorough investigation on cost definition—using actual data from operating vessels or different sources—is required to draw more nuanced conclusions on this front, which the authors consider to be beyond the scope of this paper. Finally, comparing the different consequence

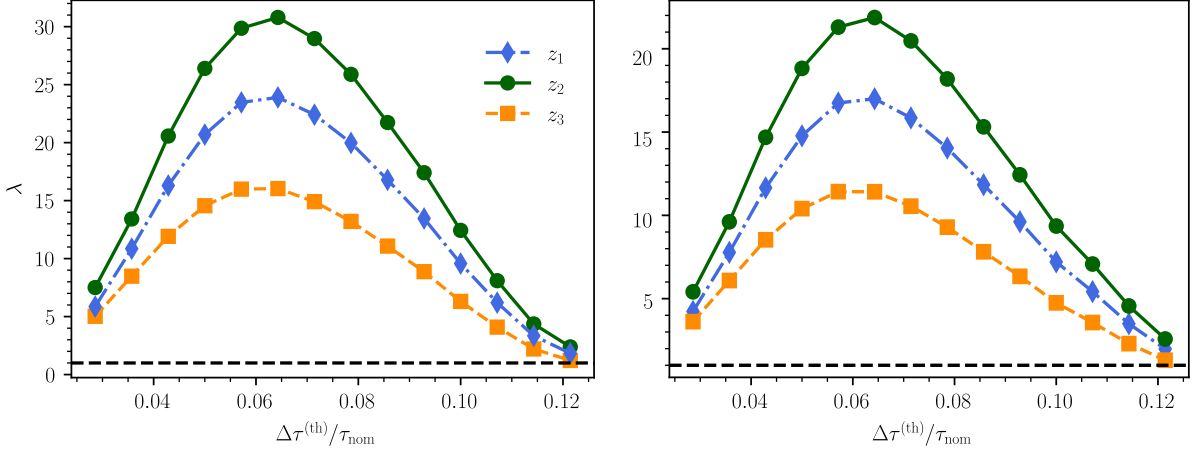


Figure 13: Expected reward to investment risk ratio as a function of the decision threshold mean value for different strain-based monitoring strategies. Left panel corresponds to  $\mathcal{R}_1(d_1)$  and right panel to  $\mathcal{R}_2(d_1)$ .

cost definitions confirms the initial interpretation of the risk profile attributed to each case, with the risk-seeker ( $\mathcal{R}_1(d_1)$ ) having the potential to enjoy greater maximum rewards. However we must note that, crucially, the marginal behaviour of the expected reward to risk ratio is similar regardless of risk profile, which showcases the potential overall benefit of acquiring monitoring information.

#### 4.4. Investigating cost margins justifying monitoring

To further investigate the effect of the intrinsic cost on the potential value of strain-based CITL monitoring, we have calculated the expected reward to investment risk ratio over a wider range of  $\mathcal{C}(z_i)$  and  $\mathcal{C}_{O\&M}(z_i)$  values. More specifically, we have assumed that  $\mathcal{C}(z_i) \in [0.1 \cdot \mathcal{C}_{\max}, 0.5 \cdot \mathcal{C}_{\max}]$  and  $\mathcal{C}_{O\&M}(z_i) = 0.01 \cdot \mathcal{C}(z_i)$  and calculated  $\lambda$  over a  $100 \times 100$  uniform grid made up of combinations of these two costs.

Results for the intermediate CITL threshold value confirm that strain-based CITL monitoring can provide benefits to maintenance planning of ship hull structures, for a wide range of intrinsic cost assignments. As the threshold increases, a non-feasible cost region emerges where  $\lambda < 1$ , which is marked by gray shading. It is noteworthy to point out that the feasible and non-feasible intrinsic cost regions are linearly separable, which is a corollary of the linear consequence cost function definition. This is a useful property of the framework as it can lead to easily interpretable decision rules for stakeholders. Finally, it is important to note that, under the same intrinsic cost assignments, the different monitoring strategies are virtually equivalent in terms of the value they add to CITL monitoring, thus further reinforcing the point made in the previous section.

The results of this procedure are presented in Figure 14 for two different CITL thresholds, one representing an intermediate CITL deterioration level and the other a more severe case. To define the extrinsic cost, we have used the risk-averse definition of the decision-to-repair consequence cost function, i.e.,  $\mathcal{R}_2(d_1)$ .

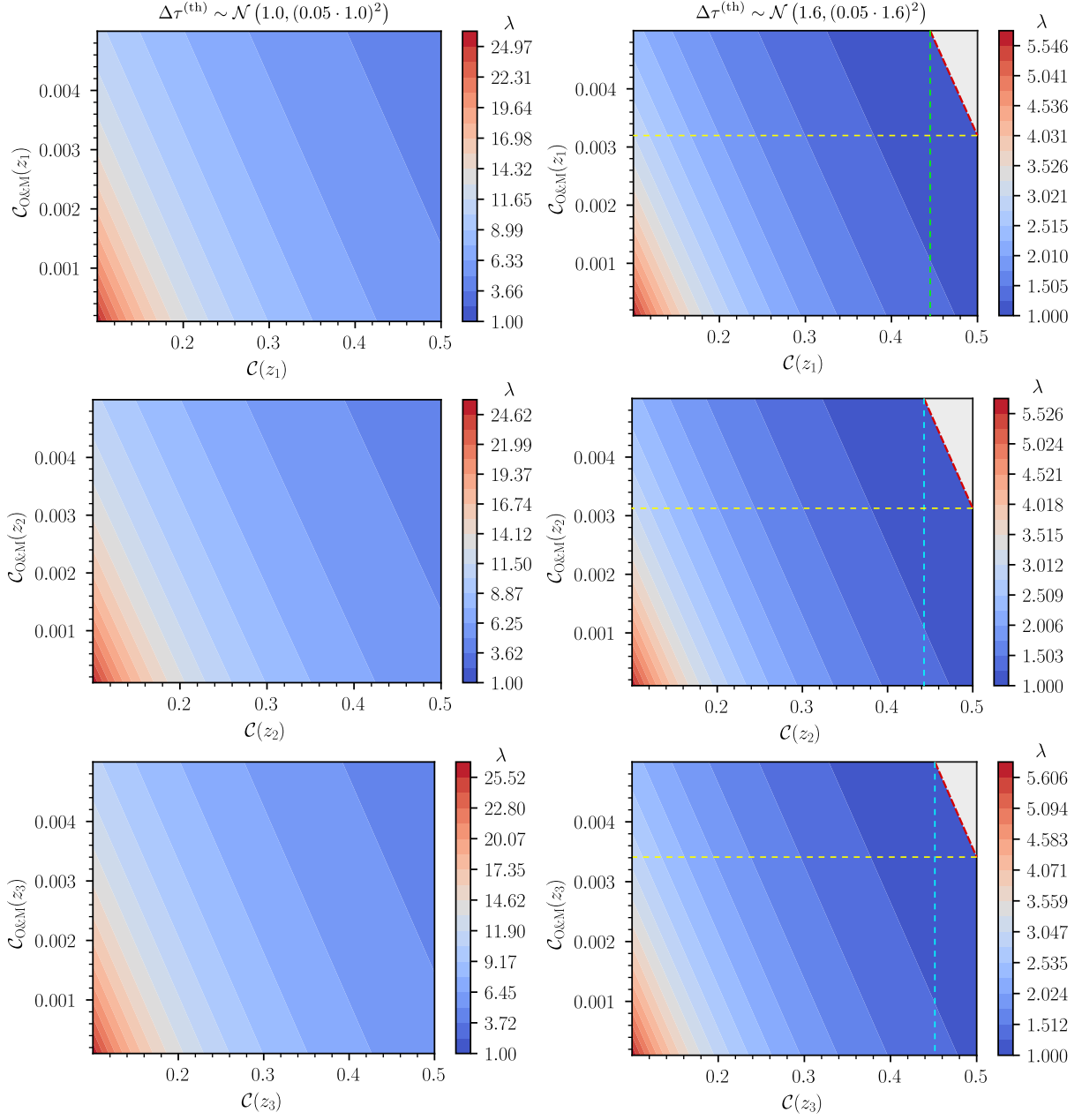


Figure 14: Expected reward to investment risk ratio maps for different intrinsic cost assignments.

#### 4.5. Investigating the utility of inspections

At this point, we have shown that strain-based CITL monitoring can be considered as a reasonable investment to assist decision-making for the maintenance planning of ship hull structures. However, to make a comprehensive assessment of its value, it must also be compared to the VoI associated with typical inspection strategies. To that end, we will use the relative risk-adjusted reward metric  $\chi(z_0, z_i)$  defined in Eq. (15), where  $z_i$  refers to the various strain-based monitoring strategies and  $z_0$  refers to the inspection-only strategy discussed earlier.

To calculate the expected reward to investment risk ratio of inspections, we have to make small adjustments to the definition of the expected lifecycle pre-posterior loss given in Eq. (11), which we will mention here for the sake of completeness. Since only one inspection takes place according to our scenario, it is assigned a dedicated intrinsic cost  $\mathcal{C}_{\text{insp}}$  and the sum defining the extrinsic cost in Eq. (11) devolves to a single term, defined as in Eq. (10). Using this adjusted expected lifecycle pre-posterior loss, the implementation in Algorithm 1 can be followed without change to estimate the VoI for inspection-only monitoring data.

The results of this comparison are presented in Figures 15 & 16 that plot the relative risk-adjusted reward between the different strain-based monitoring strategies and the inspection-only scenario for different maintenance-related CITL threshold levels. The risk-seeking profile, characterised by the decision-to-repair consequence cost  $\mathcal{R}_1(d_1)$  has been used to obtain Figure 15, while  $\mathcal{R}_2(d_1)$ —characterising the more risk-averse decision-maker—has been used to obtain Figure 16. For the strain-based monitoring strategies, the relative cost assignments discussed in Section 4.3 have been assumed here as well.

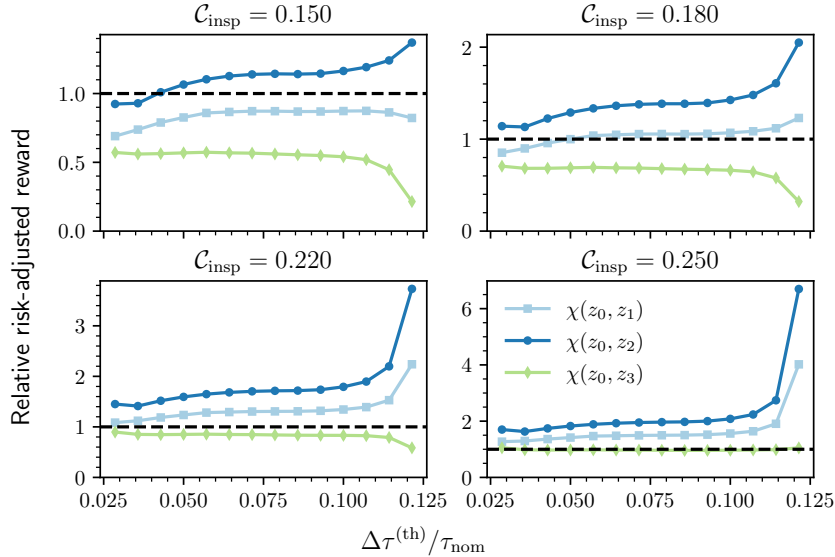


Figure 15: Relative risk-adjusted reward between strain-based monitoring strategies and inspection-only monitoring assuming consequence cost function  $\mathcal{R}_1(d_1)$ .

The black dashed line at  $\chi(z_i, z_0) = 1$  forms the boundary above which investing in strain-based monitoring is worthwhile compared to a conventional inspection-only strategy. It is important to note that this statement, as well as any other conclusions here, are valid only under the assumed inspection strategy and CITL monitoring period. Initially, we can observe that for both consequence cost function definitions and across CITL threshold values and inspection costs,  $\chi(z_i, z_0) > 0$ . This implies that, similar to strain-based monitoring (see Figure 13), investing in an inspection-only monitoring strategy can be considered as beneficial. We should note that this comes with a caveat as well, i.e., the time of inspection. Indeed, results are expected to differ if the inspection time is shifted—potentially negatively if it takes place at an earlier stage of deterioration.

Nevertheless, we can observe that the intrinsic cost of strain-based monitoring and the inspection cost are the key factors influencing which strategy is viewed as more beneficial. It is important to highlight however, that under the assumed intrinsic costs, monitoring strategy ( $z_2$ ) appears to

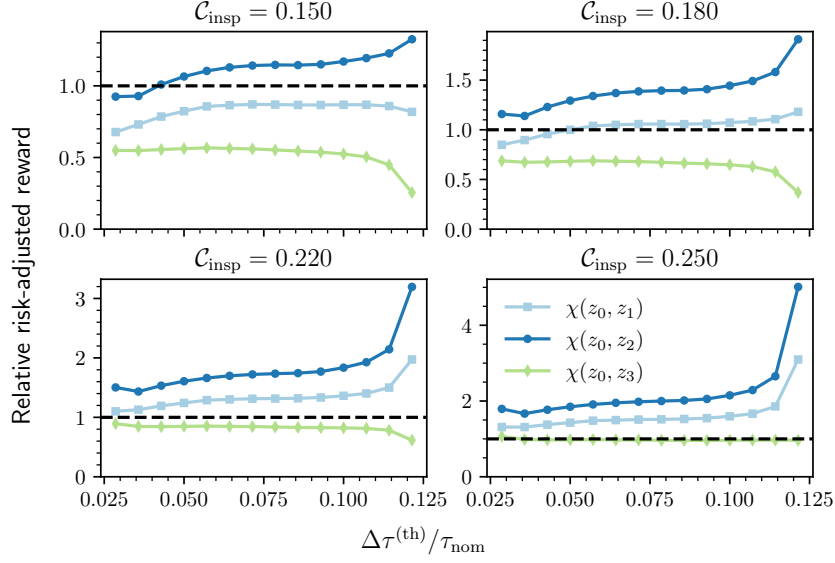


Figure 16: Relative risk-adjusted reward between strain-based monitoring strategies and inspection-only monitoring assuming consequence cost function  $\mathcal{R}_2(d_1)$ .

be preferable for the majority of scenarios. Moreover, its relative value increases as the threshold levels increase, which highlights the potential capabilities of a monitoring system that can track deterioration relatively frequently. In terms of risk-perception, we can observe that a more risk-averse decision-maker will tend to assign lower utility to strain-based monitoring. This utility, however, tends to increase as the cost of inspections is increased regardless of the risk profile.

At this point, we must concede that the cost of inspection is highly volatile, since it is affected by numerous extraneous factors, such the global trade market or shipping rates, among others. Considering all, or even a subset, of these factors is highly challenging and falls beyond the scope of this paper. However, it could become the objective of highly interesting future research.

## 5. Concluding remarks

In this work, a comprehensive assessment of the value of investing in SHM for strain-based CITL monitoring in ship hull structures was undertaken for the first time. Using Bayesian decision theory, the VoI was quantified as the expected reward to investment risk ratio for different candidate strain-based monitoring strategies as well as a conventional inspection-only scenario. The proposed framework employed exceedance probabilities, defined with respect to a maintenance-related CITL threshold, to define consequence cost functions, allowing for implicit yet interpretable modelling of decision-maker risk perception. A numerical case study was conducted, using a high-fidelity FE model of a real-world ship hull structure.

- The framework demonstrated a novel application of Bayesian decision theory to SHM for ship hull structures, introducing the VoI as a key metric.
- A definition of consequence cost functions was proposed based on an exceedance probability defined with respect to a maintenance-related CITL threshold. This definition enabled the implicit yet interpretable modelling of decision-maker risk perception.

- The numerical case study highlighted the potential value added by SHM in improving maintenance decision-making for ship hull structures.
- Results were based on rationally and heuristically defined normalised cost components, which were adapted to address the lack of comprehensive cost data.

Despite these contributions, the study is subject to certain limitations. The lack of detailed historical data on inspection and maintenance costs necessitated the use of normalised cost definitions, introducing interpretational caveats concerning the generalisability of the results. Moreover, while the binary decision set and linear consequence costs were deemed reasonable, future research should explore more realistic action/decision settings and cost function definitions.

For instance, including realistic modelling of potential repair actions and their outcomes represents a key step moving forward. A further aspect with great practical relevance is related to accounting for the potential of deteriorating or faulty sensors (see e.g., [47]). Such efforts could further establish the VoI as a practical metric for informing optimal maintenance and inspection scheduling methods across engineering structures.

### Declaration of conflicting interests

The authors declared no potential conflicts of interest with respect to the research, authorship, and/or publication of this article.

### Funding

The authors received no financial support for the research, authorship, and/or publication of this article.

### References

- [1] ABS, Advisory on structural health monitoring: The application of sensor-based approaches, 2020.
- [2] ABS, Guide for smart functions for marine vessels and offshore units, 2022.
- [3] O. Smogeli, Digital twins at work in maritime and energy, DNV GL (2017).
- [4] H. E. Torkildsen, A. Grovlen, A. Skaugen, G. Wang, A. E. Jensen, K. Pran, G. Sagvolden, Development and applications of full-scale ship hull health monitoring systems for the royal norwegian navy, 2005.
- [5] N. E. Sillionis, K. N. Anyfantis, From preventive to predictive maintenance of ship hulls: The role of shm, in: Day 2 Wed, March 08, 2023, SNAME, 2023. doi:10.5957/SOME-2023-033.
- [6] IACS, Common structural rules for bulk carriers and oil tankers, 2021.
- [7] IACS, No. 76 guidelines for assessment and repair of hull structures – bulk carriers, 2007.
- [8] J. K. Paik, J. M. Lee, J. S. Hwang, Y. I. I. Park, A time-dependent corrosion wastage model for the structures of single-and double-hull tankers and fsos and fpsos, Marine Technology and SNAME News 40 (2003) 201–217. URL: <https://doi.org/10.5957/mt1.2003.40.3.201>. doi:10.5957/mt1.2003.40.3.201.
- [9] Y. Garbatov, C. G. Soares, Risk based maintenance of deteriorated ship structures accounting for historical data, in: Advanced Ship Design for Pollution Prevention - Proceedings of the International Workshop "Advanced Ship Design for Pollution Prevention", 2010, pp. 131–147.
- [10] S. Qin, W. Cui, Effect of corrosion models on the time-dependent reliability of steel plated elements, Marine Structures 16 (2003) 15–34. doi:10.1016/S0951-8339(02)00028-X.
- [11] D. Georgiadis, M. Samuelides, A methodology for the reassessment of hull-girder ultimate strength of a vlcc tanker based on corrosion model updating, Ships and Offshore Structures 14 (2019) 270–280. doi:10.1080/17445302.2019.1577599.
- [12] C. Kim, S. Oterkus, E. Oterkus, Y. Kim, Probabilistic ship corrosion wastage model with bayesian inference, Ocean Engineering 246 (2022) 110571. doi:10.1016/j.oceaneng.2022.110571.

- [13] L. Bull, P. Gardner, J. Gosliga, T. Rogers, N. Dervilis, E. Cross, E. Papatheou, A. Maguire, C. Campos, K. Worden, Foundations of population-based shm, part i: Homogeneous populations and forms, *Mechanical Systems and Signal Processing* 148 (2021) 107141. doi:10.1016/j.ymssp.2020.107141.
- [14] J. Gosliga, P. Gardner, L. Bull, N. Dervilis, K. Worden, Foundations of population-based shm, part ii: Heterogeneous populations – graphs, networks, and communities, *Mechanical Systems and Signal Processing* 148 (2021) 107144. doi:10.1016/j.ymssp.2020.107144.
- [15] P. Gardner, L. Bull, J. Gosliga, N. Dervilis, K. Worden, Foundations of population-based shm, part iii: Heterogeneous populations – mapping and transfer, *Mechanical Systems and Signal Processing* 149 (2021) 107142. doi:10.1016/j.ymssp.2020.107142.
- [16] A. S. Katsoudas, N. E. Sillionis, K. N. Anyfantis, Structural health monitoring for corrosion induced thickness loss in marine plates subjected to random loads, *Ocean Engineering* 273 (2023) 114037. URL: <https://www.sciencedirect.com/science/article/pii/S0029801823004213>. doi:<https://doi.org/10.1016/j.oceaneng.2023.114037>.
- [17] N. E. Sillionis, K. N. Anyfantis, Optimal sensor placement for corrosion induced thickness loss monitoring in ship structures, *Marine Structures* 93 (2024) 103524. doi:10.1016/j.marstruc.2023.103524.
- [18] M. Ghasemzadeh, M. Mokhtari, A. Kefal, Localized corrosion damage prediction of steel plates in marine applications using quadrilateral inverse-shell elements based on ifem, in: E. S., S. C.G. (Eds.), *Sustainable Development and Innovations in Marine Technologies - Proceedings of the 19th International Congress of the International Maritime Association of the Mediterranean, IMAM 2022*, CRC Press/Balkema, 2023, p. 123 – 129. URL: <https://www.scopus.com/inward/record.uri?eid=2-s2.0-85145582241&doi=10.1201%2f9781003358961-17&partnerID=40&md5=72b61f58fd1fc7a068e50c7fa9669ff8>. doi:10.1201/9781003358961-17.
- [19] M. Ghasemzadeh, M. Mokhtari, M. H. Bilgin, A. Kefal, Pitting corrosion identification approach based on inverse finite element method for marine structure applications, *Ocean Engineering* 273 (2023) 113953. URL: <https://www.sciencedirect.com/science/article/pii/S0029801823003372>. doi:<https://doi.org/10.1016/j.oceaneng.2023.113953>.
- [20] M. Pozzi, A. D. Kiureghian, Assessing the value of information for long-term structural health monitoring, 2011, p. 79842W. doi:10.1117/12.881918.
- [21] D. Zonta, B. Glisic, S. Adriaenssens, Value of information: Impact of monitoring on decision-making, *Structural Control and Health Monitoring* 21 (2014). doi:10.1002/stc.1631.
- [22] S. Thöns, On the value of monitoring information for the structural integrity and risk management, *Computer-Aided Civil and Infrastructure Engineering* 33 (2018) 79–94. doi:10.1111/mice.12332.
- [23] D. Straub, E. Chatzi, E. Bismut, W. Courage, M. Döhler, M. H. Faber, J. Köhler, G. Lombaert, P. Omenzetter, M. Pozzi, S. Thöns, D. V. Val, H. Wenzel, D. Zonta, Value of information: A roadmap to quantifying the benefit of structural health monitoring, in: *ICOSSAR - 12th International Conference on Structural Safety & Reliability*, Vienna, Austria, 2017.
- [24] D. Straub, Value of information analysis with structural reliability methods, *Structural Safety* 49 (2014). doi:10.1016/j.strusafe.2013.08.006.
- [25] S. Thöns, C. Caprani, M. H. Faber, D. M. Frangopol, P. Gardoni, P. F. Giordano, D. Honfi, L. Iannacone, M. S. Khan, J. Köhler, S. Kim, N. de Koker, M. P. Limongelli, S. Miraglia, J. S. Nielsen, M. Pandey, C. Viljoen, On information value and decision analyses, *Structural Safety* 113 (2025) 102481. doi:10.1016/j.strusafe.2024.102481.
- [26] A. Kamariotis, E. Chatzi, D. Straub, N. Dervilis, K. Goebel, A. J. Hughes, G. Lombaert, C. Papadimitriou, K. G. Papakonstantinou, M. Pozzi, et al., Monitoring-supported value generation for managing structures and infrastructure systems, *Data-Centric Engineering* 5 (2024). doi:10.1017/dce.2024.24.
- [27] A. Kamariotis, E. Chatzi, D. Straub, Value of information from vibration-based structural health monitoring extracted via bayesian model updating, *Mechanical Systems and Signal Processing* 166 (2022) 108465. doi:10.1016/J.YMSSP.2021.108465.
- [28] A. Kamariotis, E. Chatzi, D. Straub, A framework for quantifying the value of vibration-based structural health monitoring, *Mechanical Systems and Signal Processing* 184 (2023) 109708. doi:10.1016/j.ymssp.2022.109708.
- [29] P. F. Giordano, L. J. Prendergast, M. P. Limongelli, A framework for assessing the value of information for health monitoring of scoured bridges, *Journal of Civil Structural Health Monitoring* 10 (2020) 485–496. doi:10.1007/s13349-020-00398-0.
- [30] M. Chadha, Z. Hu, M. D. Todd, An alternative quantification of the value of information in structural health monitoring, *Structural Health Monitoring* 21 (2021) 138–164. URL: <https://doi.org/10.1177/14759217211028439>, doi: 10.1177/14759217211028439.

- [31] M. Chadha, M. K. Ramancha, M. A. Vega, J. P. Conte, M. D. Todd, The modeling of risk perception in the use of structural health monitoring information for optimal maintenance decisions, *Reliability Engineering & System Safety* 229 (2023) 108845. doi:10.1016/j.ress.2022.108845.
- [32] M. Chadha, Z. Hu, C. R. Farrar, M. D. Todd, A value-of-information-based optimal sensor placement design framework for cost-effective structural health monitoring (with application to miter gate monitoring), *Structural Health Monitoring* (2024). doi:10.1177/14759217241275643.
- [33] J. S. Nielsen, D. Tcherniak, M. D. Ulriksen, A case study on risk-based maintenance of wind turbine blades with structural health monitoring, *Structure and Infrastructure Engineering* 17 (2021) 302–318. doi:10.1080/15732479.2020.1743326.
- [34] S. Cantero-Chinchilla, J. Chiachío, M. Chiachío, D. Chronopoulos, A. Jones, Optimal sensor configuration for ultrasonic guided-wave inspection based on value of information, *Mechanical Systems and Signal Processing* 135 (2020) 106377. URL: <https://www.sciencedirect.com/science/article/pii/S0888327019305989>. doi:<https://doi.org/10.1016/j.ymssp.2019.106377>.
- [35] A. Kamariotis, L. Sardi, I. Papaioannou, E. Chatzi, D. Straub, On off-line and on-line bayesian filtering for uncertainty quantification of structural deterioration, *Data-Centric Engineering* 4 (2023). doi:10.1017/dce.2023.13.
- [36] E. Simoen, G. D. Roeck, G. Lombaert, Dealing with uncertainty in model updating for damage assessment: A review, *Mechanical Systems and Signal Processing* 56-57 (2015) 123–149. doi:10.1016/j.ymssp.2014.11.001.
- [37] D. G. Georgiadis, M. S. Samuelides, The effect of corrosion spatial randomness and model selection on the ultimate strength of stiffened panels, *Ships and Offshore Structures* 16 (2021) 140–152. URL: <https://doi.org/10.1080/17445302.2021.1907063>. doi:10.1080/17445302.2021.1907063, doi: 10.1080/17445302.2021.1907063.
- [38] D. Cristiani, C. Sbarufatti, F. Cadini, M. Giglio, Fatigue damage diagnosis and prognosis of an aeronautical structure based on surrogate modelling and particle filter, *Structural Health Monitoring* 20 (2021) 2726–2746. doi:10.1177/1475921720971551.
- [39] M. K. Ramancha, M. A. Vega, J. P. Conte, M. D. Todd, Z. Hu, Bayesian model updating with finite element vs surrogate models: Application to a miter gate structural system, *Engineering Structures* 272 (2022) 114901. URL: <https://www.sciencedirect.com/science/article/pii/S0141029622009798>. doi:<https://doi.org/10.1016/j.engstruct.2022.114901>.
- [40] N. E. Sillionis, K. N. Anyfantis, A hierarchical bayesian approach for parameter identification in structural deterioration models using probabilistic surrogate models, *e-Journal of Nondestructive Testing* 29 (2024). doi:10.58286/29571.
- [41] S. Brooks, A. Gelman, G. Jones, X.-L. Meng, *Handbook of Markov Chain Monte Carlo*, Chapman and Hall/CRC, 2011. doi:10.1201/b10905.
- [42] M. D. Hoffman, A. Gelman, The no-u-turn sampler: adaptively setting path lengths in hamiltonian monte carlo, *J. Mach. Learn. Res.* 15 (2011) 1593–1623. URL: <https://api.semanticscholar.org/CorpusID:12948548>.
- [43] M. Betancourt, A conceptual introduction to hamiltonian monte carlo, 2017.
- [44] E. Bingham, J. P. Chen, M. Jankowiak, F. Obermeyer, N. Pradhan, T. Karaletsos, R. Singh, P. A. Szerlip, P. Horsfall, N. D. Goodman, Pyro: Deep universal probabilistic programming, *J. Mach. Learn. Res.* 20 (2019) 28:1–28:6. URL: <http://jmlr.org/papers/v20/18-403.html>.
- [45] D. Phan, N. Pradhan, M. Jankowiak, Composable effects for flexible and accelerated probabilistic programming in numpyro, 2019.
- [46] A. Vehtari, A. Gelman, D. Simpson, B. Carpenter, P.-C. Bürkner, Rank-normalization, folding, and localization: An improved  $\hat{r}$  for assessing convergence of mcmc (with discussion), *Bayesian Analysis* 16 (2021). doi:10.1214/20-BA1221.
- [47] Y. Yang, M. Chadha, Z. Hu, M. D. Todd, An optimal sensor design framework accounting for sensor reliability over the structural life cycle, *Mechanical Systems and Signal Processing* 202 (2023) 110673. doi:10.1016/j.ymssp.2023.110673.